International Biodeterioration & Biodegradation 215 (2026) 106455

Contents lists available at ScienceDirect

International Biodeterioration & Biodegradation

journal homepage: www.elsevier.com/locate/ibiod

Quantification of subaerial algae on building materials by a new standardised imaging Pulse-Amplitude-Modulation Fluorometry (PAM-F) method

Leonie Stohl [a,b], Jake Cook [a], Julia von Werder [a,*], Anna A. Gorbushina [a,c], Chiara Tonon [a]

[a] Bundesanstalt für Materialforschung und -prüfung (BAM), Unter den Eichen 87, Berlin, 12205, Germany
[b] Karlsruher Institut für Technologie, Institut für Massivbau und Baustofftechnologie, Baustoffe und Betonbau, MPA Karlsruhe, CMM Karlsruhe, Gotthard-Franz-Str., Karlsruhe, 376131, Germany
[c] Freie Universität Berlin, Fachbereich Geowissenschaften, Institut für Geologische Wissenschaften, Malteserstraße 74-100, 12249 Berlin, Germany

ARTICLE INFO

Keywords:
Subaerial Biofilm (SAB)
Bioreceptivity
Concrete and marble substrates
Non-destructive testing
Quantitative fluorescence imaging
Automated data processing
Python-based algorithm

ABSTRACT

Imaging Pulse-Amplitude-Modulation Fluorometry (PAM-F) is a quantitative, sensitive, and non-destructive tool for detecting early biofilm establishment, yet its broader use has been limited by the lack of standardised protocols and by uncertainties arising from material-specific effects. In this study, the first comprehensive protocol is presented considering substrate properties and achieving reproducible dark fluorescence yield (F_0) measurements even for low algal cell densities. Our workflow combines standardised sample preparation with an algorithm-driven evaluation to generate calibration curves, detection limits, and optimal device settings. By applying two defined inoculation ranges of the subaerial green alga *Jaagichlorella* sp. AB13.021D5 to marble and concrete pellets, and polycarbonate membranes, we show that F_0 intensity reflects not only algal abundance and device settings but also physical and mineralogical substrate properties. Particularly the high reflectance of marble increased noise and oversaturation effects, demonstrating the necessity of substrate-specific calibration. This transferable protocol establishes *Jaagichlorella* sp. AB13.021D5 as a test organism for comparative and application-oriented bioreceptivity studies (such as evaluating material susceptibility, comparing protective treatments, and monitoring early colonisation). By delivering validated measurement settings as well as substrate-specific calibration curves and detection limits for Imaging PAM-F studies, this work closes a critical methodological gap and supports the development of evidence-based biodeterioration management strategies.

1. Introduction

Subaerial biofilms (SABs) are densely packed microbial communities. They form at the boundary between solid surfaces and the atmosphere, and their remarkable ability to endure extreme stress enables them to thrive even in the harshest conditions, making them ubiquitous colonisers of terrestrial environments (Gorbushina, 2007; Villa et al., 2016). Their ability to colonise surfaces depends on different intrinsic and extrinsic factors, such as the species involved, the environmental conditions, and the material bioreceptivity, defined as its aptitude to be colonised by (micro-)organisms (Guillitte, 1995; Sanmartín et al., 2021b).

The growing interest in research on bioreceptivity (Sanmartín et al., 2021b) has generated a clear demand for standardised, reproducible methodologies that enable reliable comparisons across studies (Stohl et al., 2023). Research on SABs developing on mineral surfaces generally aims to support the development of materials with either inhibited or enhanced colonisation potential, depending on the intended application (Manso et al., 2014; Vázquez-Nion et al., 2018; Fuentes Alonso and Prieto, 2021a). In both cases, precise quantification of early stage microbial development is essential for meaningful investigations into biofilm dynamics as well as their chemical and physical interactions with the substrate (Gladis and Schumann, 2011a; Stohl et al., 2025b). Quantitative data are particularly important when developing building

* Corresponding author.
E-mail addresses: leonie.stohl@bam.de (L. Stohl), jake-thomas.cook@bam.de (J. Cook), julia.von-werder@bam.de (J. von Werder), anna.gorbushina@bam.de (A.A. Gorbushina), chiara.tonon@bam.de (C. Tonon).

https://doi.org/10.1016/j.ibiod.2026.106455
Received 2 April 2026; Received in revised form 14 August 2026; Accepted 19 August 2026
Available online 1 September 2026

materials, as they must meet certain standards and fulfil reproducible, quantifiable performance parameters to be approved for construction (Contreras et al., 2011; Cheng, 2013).

Traditionally, building materials are developed to exhibit very low bioreceptivity in order to preserve a clean and visually homogeneous appearance (De Muynck et al., 2009; Maury-Ramirez et al., 2013; Dalod et al., 2014; Pinheiro et al., 2019; Santo et al., 2021). However, a complementary trend has emerged over the past decade: the intentional design of highly bioreceptive materials for ecological and aesthetic applications, such as vertical greening and biodiversity-driven architecture (Manso and Aguado, 2016; Veeger et al., 2021a; Elgaali et al., 2024; Jakubovskis, 2024).

In parallel, bioreceptivity assessments and SAB monitoring remain central in the field of cultural heritage conservation, where understanding and preventing biodeterioration processes is essential for safeguarding historical stone, concrete, and composite surfaces (Cutler et al., 2013; Villa et al., 2016; Cappitelli et al., 2020; Fuentes Alonso and Prieto, 2021a; Zhu et al., 2023; Prieto et al., 2024).

Across these varied application contexts, including protective engineering, green urban design, and heritage conservation, robust, sensitive, and standardised methodologies for quantifying the early stages of microbial colonisation are essential.

Understanding the mechanisms behind the establishment and development of SABs is fundamental for bioreceptivity studies. Reliable analysis of the earliest colonisation stages requires a non-destructive, sensitive analytical tool capable of detecting and quantifying low microbial biomass. For photosynthetic organisms, chlorophyll fluorescence fulfils these requirements since its discovery in the 1930s (Kautsky and Hirsch, 1931; Rosenqvist and van Kooten, 2003). The technique advanced significantly with the introduction of Pulse-Amplitude-Modulation Fluorometry (PAM-F) in the 1980s (Schreiber et al., 1986), which allowed for more precise monitoring of vitality, growth and physiological responses of photosynthetic organisms (Baker, 2008; Eggert et al., 2006; Najafpour, 2012; Oxborough, 2004; Sanmartín et al., 2020b; Stock et al., 2019). Since then, a range of PAM-F devices has been developed for applications such as *in vivo* fluorescence measurements in microalgal cultures (Figueroa et al., 2013) and comparative physiological characterisation of strains under different stressors (Karsten and Rindi, 2010; Karsten et al., 2014, 2016).

PAM-F has demonstrated strong potential for bioreceptivity studies, having been successfully applied to detect early-stage colonisation, as well as to monitor photosynthetic biofilms under controlled and natural conditions (Eggert et al., 2006; Gladis and Schumann, 2011b; von Werder and Venzmer, 2013; Sanmartín et al., 2020a). However, its broader application is hindered by inconsistent reporting practices and a lack of shared methodological standards (Nies et al., 2021). Comparability is limited by device-specific differences, including optical systems, working distance, light wavelength and intensity, and software configuration, as well as the absence of absolute physical units for expressing measured signal intensities (Eggert et al., 2006; Nielsen and Nielsen, 2008; Vieira et al., 2013). Even when the same device type is used, variability in measurement settings strongly influence outcomes, and published studies often omit the documentation required for reproducibility (Nies et al., 2021).

Moreover, external parameters such as ambient light, temperature and water availability influence the photosynthetic activity itself (Schreiber, 2004; Häubner et al., 2006; Manso et al., 2014; Sjollema et al., 2014), and by that, PAM-F measurement quality and detection limits. Among these factors, water availability has the greatest impact on photosynthetic activity in SABs. Desiccation causes a progressive inhibition of photosynthetic activity that differs between strains, while rehydration allows rapid recovery (Häubner et al., 2006; Karsten et al., 2014, 2016). Irradiance plays an indirect role, as increasing solar radiation accelerates surface water evaporation, driving desiccation and inducing measurable stress in the photosynthetic microorganisms (Häubner et al., 2006). Temperature, while influencing photosynthetic oxygen production at extremes, was not identified as a primary limiting factor for photosynthesis under field conditions (Häubner et al., 2006; Karsten et al., 2016).

As PAM-F measurements reflect the physiological state of the photosynthetic apparatus, all factors influencing photosynthesis will inherently be captured in the fluorescence signal, underlining the importance of controlled and standardised measurement conditions when using PAM-F for quantitative assessments.

Importantly, the substrates themselves can impact PAM-F measurements in multiple ways (Eggert et al., 2006; Carpentier et al., 2013; von Werder and Venzmer, 2013; Wangpraseurt et al., 2019), but their effect is often neglected. For example, Carpentier and colleagues (2013) addressed the variable chlorophyll fluorescence signal intensity detected for cyanobacteria, green algae and diatoms on a wide range of stones, highlighting how reflective substrates tended to increase signal intensity measured with PAM-F. A similar effect was also described by Wangpraseurt and colleagues (2019) for green algae examined in planar hydrogel systems simulating coral skeletons. Moreover, substrate porosity is another crucial factor, as it directly affects wettability and water availability.

Although shared protocols and calibration curves would allow cross-comparison of experimental data, until this moment few efforts have focused on this. Models correlating chlorophyll fluorescence signals measured with PAM-F with subaerial algal cell density already exist (Eggert et al., 2006; Manso et al., 2015), however only few studies have systematically explored calibration curve construction (Eggert et al., 2006; von Werder and Venzmer, 2013; Stock et al., 2019). Moreover, to date no published studies have detailed a methodology for testing device software settings that enables unbiased and automated selection of these settings as an integral component of the calibration process.

Among available PAM-F devices (Figueroa et al., 2013), Imaging PAM-F is considered the most suitable for studying spatially heterogeneous algal growth (Eggert et al., 2006; von Werder and Venzmer, 2013). Quantitative use of Imaging PAM-F requires calibration curves that establish a correlation between algal cell density and the correlating chlorophyll fluorescence signal (F_0), however only few attempts have been made. Eggert et al. (2006) tested two PAM-devices and three measurement settings combinations on five subaerial algal strains to obtain calibration curves and detection limits through correlating F_0 signal intensity to chlorophyll content. Manso (2014) implemented a similar calibration approach and highlighted limitations of correlating F_0 signals with commonly used indirect methods for estimating algal abundance. Most of the commonly used methods employed for algal cell density estimation aimed at building calibration curves with F_0-values rely on spectroscopic analyses, either *in vivo*, such as optical density (Nikolaou et al., 2015; Rousso et al., 2022) and chlorophyll autofluorescence (Schagerl et al., 2022), or in vitro, such as by quantification of chlorophyll-a extracted from a known sample (Sanmartín et al., 2017, 2020c). Other widespread reference methods are the measures of dry and wet weight. However, many of these techniques hold potentially limiting factors for their accuracy, such as the solvent used for chlorophyll extraction (Castle et al., 2011), the low sensitivity for low cell concentrations, or the impact of filtering phase for dry weight (Schagerl et al., 2022). Moreover, culturing conditions and growth phase are known factors that influence both chlorophyll-a content and photosynthesis reaction centres efficiency (Qiu et al., 2013; Main et al., 2014; Stock et al., 2019), which, in multiple ways, affect the PAM-F signals including those used as proxies for algal cell density.

A standardised, quantitative approach for using Imaging PAM-F in building material bioreceptivity studies would therefore offer substantial benefits. In this study, we (i) developed a reproducible protocol for generating algal cell density-F_0 calibration curves, covering cultivation, sample preparation, and measurement configuration, and incorporating a systematic exploration of software settings. To further enhance objectivity, (ii) we implemented a customisable, data-driven evaluation algorithm to automatically identify the most reliable settings for

calibration curve construction. Using a recently isolated representative SAB phototrophic organism and three different substrates, we additionally assessed (iii) the suitability of the green alga *Jaagichlorella* sp. for highly standardised analyses and (iv) determined the influence of substrate optical and physical properties on Imaging PAM-F signal intensity.

2. Materials and methods

2.1. Imaging PAM-F device

When a photosynthetic organism is exposed to excitation light, photons are absorbed by the Photosynthetic System II (PSII) antennas, and the excitation energy is transferred to the PSII reaction centres. There, the excitation energy can be dissipated as heat, emitted as fluorescence, or used to drive photochemistry. In the photochemical pathway, charge separation occurs at electron donor P680, leading to electron transfer to the primary acceptor Q_A. The oxidised reaction centre $P680^+$ is then reduced by electrons derived from water splitting at the oxygen-evolving complex, producing oxygen, protons and electrons. The extracted electrons are transported through the photosynthetic electron transport chain, where they are used to generate chemical energy for the organism's metabolism (Schreiber, 2004; Baker, 2008).

The efficiency of this process is largely dependent on the redox state of the primary electron acceptor Q_A. When Q_A is oxidised, reaction centres are considered open, allowing efficient photochemistry and resulting in low fluorescence yield. In contrast, when Q_A is reduced, reaction centres are closed, electron transfer is inhibited, and excitation energy is increasingly dissipated as fluorescence and heat (Genty et al., 1989). PAM fluorometry utilises this effect by applying a weak modulated measuring light (ML), which tracks fluorescence continuously without driving photochemistry, and periodic saturating pulses (SP) that transiently close all reaction centres, providing estimates of PS II quantum yield and energy dissipation (Genty et al., 1989; Schreiber, 2004; Baker, 2008).

Among the various parameters recorded by PAM-F devices, SAB studies commonly focus on the parameters F_0 and F_v/F_m. The dark fluorescence yield F_0 is the minimum fluorescence emitted in the dark adapted state, when P680 is open and fully oxidised (Schreiber, 2004). It is measured with a weak ML that does not induce PSII centre closure and is expressed in relative fluorescence units. Because F_0 correlates to chlorophyll-a associated with PSII, it scales with photosynthetic biomass and is frequently used as a proxy to record growth (Stock et al., 2019). In contrast, the F_v/F_m parameter describes the maximal PSII quantum yield under dark-adapted conditions and serves as an indicator of the physiological state of the organism. F_v/F_m is calculated using the maximum fluorescence yield (F_m; Schreiber, 2004), obtained after closing all PSII reaction centres with a short, intense light impulse (Saturation Pulse, SP), together with the F_0 parameter:

$$\frac{F_v}{F_m} = \frac{(F_m - F_0)}{F_m} \quad [1]$$

Because it reflects PSII efficiency, F_v/F_m is commonly used as a proxy for physiological stress. When stress gets too severe, PSII reaction centres become damaged or downregulated, resulting in a measurable decline in F_v/F_m that signals the onset of photoinhibition (Maxwell and Johnson, 2000). In SAB research, such decreases have been documented in response to stressors including desiccation, excessive irradiance, and biocide exposure (Häubner et al., 2006; Tretiach et al., 2010; von Werder and Venzmer, 2013).

This study used a MINI Version IMAGING-PAM M-Series (Heinz Walz GmbH, Effeltrich, Germany) equipped with a blue measurement head (IMAG-MIN/B), and matching camera (IMAG-K6) and objective (K6/MIN). The LED array used to generate the light impulses comprised 12 LEDs arranged in four groups of three. The emission spectra and corresponding light intensities are provided in Appendix (S1 and S2).

The device runs on the software ImagingWin v2.56zn, specific for Imaging PAM-F devices from this producer. The software offers a wide range of adjustable measurement settings, that can be classified in two categories, light regulation and software calculation parameters (Table 1).

For measurements, the SP and Measuring Light Frequency parameters were set to 1, the Saturation Pulse Width to 4×60ms and the Damping factor at 2. Absorptivity settings were Red Gain 1, Red Intensity 25, and NIR 3. External light, actinic light, and booster were not applied. Moreover, the software for this Imaging PAM fluorometer allows adjustment of the recorded fluorescence signal through the software parameter Gain (G), a computational amplification factor applied to the detected fluorescence signal that scales the output without altering the underlying photosynthetic process.

As studies with similar scopes and devices state ML and G to be the most influential software settings (Eggert et al., 2006; von Werder and Venzmer, 2013; Stock et al., 2019), these parameters were the selected and systematically varied in this study. From here on, the term "software measurement setting" refers to specific combinations of ML and G, as further defined in the details of the experiments (see Sections 2.5 and 2.6). To minimise external light influences, the Imaging PAM-F device was covered with a black cloth during data acquisition. After each measurement, samples were returned to dark acclimation for another 20 min before the next measurement.

This Imaging-PAM-F device acquires fluorescence data over an area of 32 mm × 24 mm and measurement files include a visual mapping of the recorded signals. The software facilitates the placement of single or multiple selection areas (areas of interest; AOIs) of any size and shape and then extracts information over set AOIs, allowing for a point-specific data extraction and a comparison between different AOIs. Fluorescence data were extracted with the ImagingWin software by implementing AOIs of equal size. The size of the AOIs is selected to fit the largest F_0 signal area within, while keeping them small enough to exclude F_0 signal values from adjacent inoculations, and allowed assessment of how substrate properties, software measurement settings, and concentration range influence F_0 signal intensities (Fig. 1).

Data were obtained through the mode recommended for spatially heterogenous algal growth, which calculates the average F_0 signal intensity for all pixels within the selected AOI that show both a F_0, and a corresponding F_v/F_m signal intensity above 0. The resulting average F_0 signal intensity corresponds to areas with photosynthetic activity only, effectively filtering out areas without any F_0 signal intensity as well as measurement noise. The obtained signal intensities are expressed in an arbitrary unit with values ranging between 0 and 1.

2.2. Algal material

The test organism *Jaagichlorella* sp. (AB13.021D5, provided by Andreas Beck; Research Collection of the Botanische Staatssammlung München, SNSB-BSM) is a green coccoid alga isolated from a North-West exposed outdoor wall in Berlin (Germany). It was selected as a representative local coloniser of urban building façades, especially those in sheltered and shaded locations not exposed to direct sunlight, making it a relevant organism for realistic bioreceptivity assessments.

As an algal strain originating from a building surface, the organism is of ecological relevance and expected to be capable of colonising a range of building materials, which is consistent with its application in controlled bioreceptivity testing across the different substrates investigated in this study. Furthermore, the strain is representative of a broader group of subaerial green algae that share similar morphological, physiological, and ecological characteristics.

The strain grows reliably under laboratory conditions, and its moderate growth rate and unicellular morphology also facilitate controlled quantification of biomass and physiological activity.

To develop biomass, the alga was cultivated in liquid culture (Bold's

Table 1
PAM settings.

	Settings	Description	Preliminary experiments	Calibration experiments
Light regulation parameters	**Measuring Light Intensity**	Determines the intensity of the pulse-modulated measuring light for fluorescence detection.	+	+
	Measuring Light Frequency	Sets the pulse frequency of the measuring light.	+	-
	Actinic Light Intensity and Width	Controls the temporal width and light intensity used to drive photosynthesis.	-	-
	Saturation Pulse Intensity	Defines the intensity of the saturation pulse used to saturate PSII reaction centres.	+	-
	Saturation Pulse Width	Controls the temporal width of the saturation pulse used to saturate PSII reaction centres.	-	-
	External Light Intensity and Width	Switches external light sources on or off, with configurable light intensity and temporal width.	-	-
	Booster	Temporarily maximizes the LED-current during the Saturation Pulse width for better detection of weakly fluorescing samples.	-	-
Software calculation parameters	**Gain**	Determines the amplitude of the fluorescence signal.	+	+
	Damping	Smooths the signal, reducing noise at the cost of response speed.	+	-
	Absorptivity	Defines the fraction of incident PAR assumed to be absorbed.	-	-

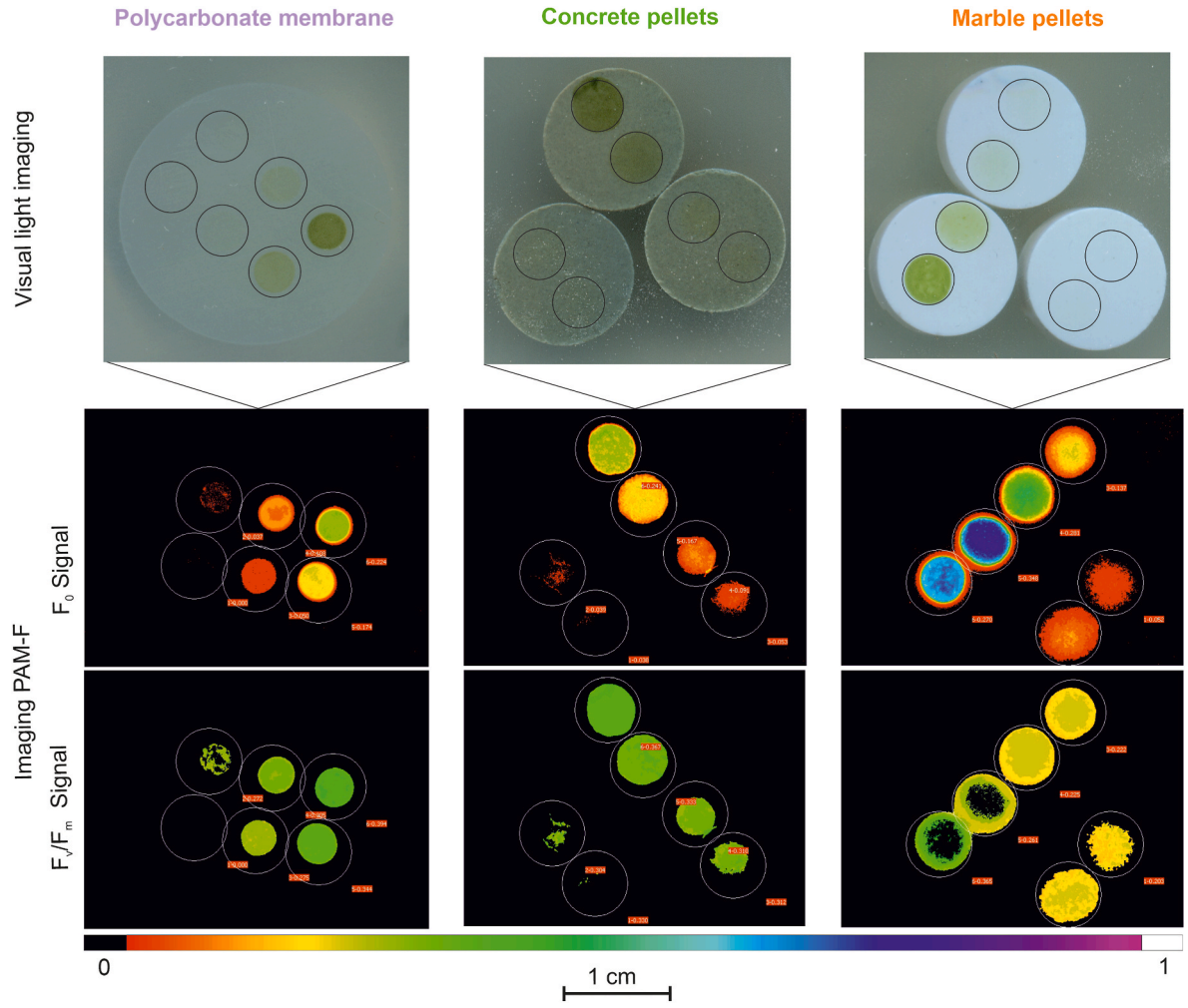

Fig. 1. Illustration of the method for inoculation and data extraction. The first row shows visual light imaging of the three substrates inoculated with 10 µL of six highly concentrated algal suspensions. The two highest concentrations are well visible with visual light imaging, whereas the remaining four are less evident. Below, the respective F_0 and F_v/F_m signal intensities are visualized in the Imaging PAM-F measurement files. The measurements were carried out with same setting for all substrates. All set AOIs (white circles) are of the same size to enable a direct comparison within a sample as well as between samples. The materials display an influence on the fluorescence signal area and intensity.

Basal Medium, BBM) in controlled conditions in a shaker (Kuhner Shaker ISF1-X; Birsfelden, Switzerland; shaking 100 rpm,temperature of 20°C) in white light, with 12/12 h day/night controlled with a photoperiod and irradiation control system (PhotoBiosim PBCON-24T-700-4, DesignInnova; New Delhi, India) set to obtain a photon flux density of ~100 µmol photons m-2s-1. In preparation for the

experiment, the microorganism was inoculated from the planktonic culture on BBM plates in a concentration of 10^6 cells/cm^2 and cultivated for about two weeks in a climatic chamber (Percival CU-22L, Percival-Scientific; Perry, IA, USA) equipped with cool white fluorescent lamps (Philips F17T8, 17W; Amsterdam, The Netherlands) in controlled conditions (12/12 h day/night, temperature of 18°C, photosynthetic photon flux density ~10 μmol photons $m^{-2}s^{-1}$). Immediately before the experiment, the algal cells were harvested from the plates and suspended in water at the desired concentrations (see Section 2.4).

2.3. Material substrates

The experiments were carried out on substrates relevant to common testing and growth situations. Polycarbonate membranes, often employed as substrates for biofilm formation and development studies (Singla et al., 2014; Sanmartín et al., 2021a; Baishya, 2024), represent inert, neutral substrates with a very defined porosity. Mineral pellets are made by compacting finely ground and sifted powder of defined origin to obtain standardised substrates particularly suitable for weathering and bioreceptivity tests (Tonon et al., 2021). Concrete pellets are a relevant reference due to the widespread use of cementitious building materials (Nilimaa, 2023; Vijay et al., 2025; Xiao et al., 2025). Marble pellets stand for the wide interest in marble and calcareous stones in cultural heritage context (Miller et al., 2009, 2012; Pinheiro et al., 2019).

The polycarbonate membranes employed in this study have a diameter of 25 mm and a pore size of 0.2 μm (Sartorius Polycarbonate Track Etch Membrane Filters, Fisher Scientific). As mineral substrates, white Carrara marble (Carrara, MS, Italy) and a conventional concrete mix (CEM I, w/c 0.6, CEN standard sand according to EN 196-1) were selected and processed to produce standardised pellets following the preparation described by Tonon et al. (2021). Pellets with a mass of 890 mg and a diameter of 13 mm were produced using a VANEOX 15 t Press MANUAL (FLUXANA GmbH & Co. KG, Germany). A pressure of 7.85 tons was applied. The pellet manufacturing ensured homogeneous samples with comparable surface properties, allowing a direct comparison of different materials with a high degree of standardisation. No chlorophyll fluorescence signal was detected from the sterile surface of all the materials, regardless of their moisture content.

For an in depth understanding of the interaction between algal inoculate, substrates and Imaging PAM-F device, material properties of the substrates were assessed.

Wettability was assessed on five replicates per material. Water contact angle measurements were performed using an optical contact angle goniometer (OCA 35XLH, DataPhysics, Germany). A droplet volume of 3 μl deionised water was applied to the substrate surface, and the contact angle was recorded after 10 s.

Color measurements were carried out in triplicate to determine L*a*b* values and reflectance using a handheld spectrophotometer (Ci62L, X-Rite GmbH, Germany). Data were recorded and processed using the associated software (Color iQC Professional, X-Rite GmbH, Germany). Samples were measured in a plated, humid state through the lid of the Petri dish, ensuring optical conditions comparable to those during Imaging PAM-F measurements. For the transparent polycarbonate membranes, opacity was additionally determined.

The pH values of the materials in contact with liquid water were assessed using a method adapted from Stohl et al. (2025a). The materials were placed in containers and combined with 2 ml of deionised water. The pH measurements were taken over time, with the measurement after 24 h corresponding to the pre-acclimation period of the pellets prior to inoculation (see Section 2.4). Measurements were conducted using a pH electrode connected to a data logger (WTW SenTix 41 and WTW pH 3310; Xylem Analytics Germany Sales GmbH & Co. KG, Germany).

Porosity of the mineral substrates was assessed in five replicates using gas pycnometry (AccuPyc 1330, Micromeritics GmbH, Germany) combined with a bulk-density-derived volume approach. This method quantifies the helium-accessible porosity, the fraction of fine, open pores within the material.

2.4. Sample preparation

The samples used for both algal-substrate compatibility assessment (see Section 2.5) and calibration experiments (see Section 2.6) were prepared prioritising highly controlled conditions such as sterility of the materials and standardised inoculation procedures. Inoculations with axenic *Jaagichlorella* sp. cultures mitigate the risk of non-photosynthetic organisms shading chlorophyll fluorescence and ensure fluorescence signals originate from a single algal strain, avoiding Chl/F variability associated with mixed populations and improving quantification reliability (Jakob et al., 2005). To maintain controlled, axenic conditions, substrates, agar, and additional materials were autoclaved. Substrates were plated on agar 24 h prior to inoculation and measurement, to allow water absorption up to saturation by the substrates.

Algal material was scraped from the plates and washed in water three times through centrifugation to eliminate dead cells and debris and separate clumps of cells. Algal concentrations were obtained by dilution of this algal suspension after through centrifugation and manual cell counting using a Thoma chamber (Dökümcüoğlu and Yılmaz, 2020). The inoculation on the substrates was carried out by dropping 5 μl of algal suspension from a height of 1-2 cm from the surfaces. After inoculation, samples were shortly left in the clean bench environment to allow complete drying of the suspension drop, and then the plates were sealed with parafilm to ensure consistent humidity. Each sample consisted of a material inoculated with the algal concentrations to be tested in the respective experiment. Including multiple concentrations within a single measurement increased efficiency and improved data quality, as all concentrations within a concentration range were measured under identical conditions.

Before each measurement with Imaging PAM-F, samples underwent a 20-min dark acclimation period, following the established practice for chlorophyll fluorescence measurements (Eggert et al., 2006; Stock et al., 2019; Sanmartín et al., 2020a).

2.5. Algae-substrate compatibility assessment

When transferring algae from water-rich media (BBM) to solid surfaces, cellular physiological transitions impacting the PAM-F signals are to be expected, even in the very first hours from the inoculation (Li et al., 2024). As some hours are required to measure algal concentrations with multiple settings, the substrate-microorganism compatibility should be verified to ensure data reliability. This is particularly true in the case of toxic substrates, which can inhibit biofilm development (Li et al., 2017; Komar et al., 2025).

To assess the compatibility between material substrate and *Jaagichlorella* sp., an algal viability experiment was performed. Compatibility was defined as the stability of algal chlorophyll fluorescence signals over the extended measurement period required for the calibration experiment, with F_0 stability serving as the primary criterion. Because the measurements were acquired using the mode recommended for spatially heterogeneous algal growth (see Section 2.1), the calculated F_0 values may be affected by changes in the spatial extent of the F_v/F_m signal, although not by changes in its intensity. Therefore, the temporal stability of both the F_0 signal intensity and the F_v/F_m signal area was assessed. F_v/F_m signal area was analysed using ImageJ (Schneider et al., 2012) and expressed as the percentage of the measured area covered by the fluorescence signal (area-%).

The different substrates were inoculated with 5 μL of suspensions containing 10^6 and $10^{6.25}$ algal cells/ml, resulting in $5.00 \cdot 10^3$ and $8.89 \cdot 10^3$ algal cells/AOI deposited on the materials. The samples were measured in quadruplicate over 8 h, always using a fixed software measurement setting (ML 5, G3).

2.6. Imaging PAM-F calibration experiment

The calibration experiment presents a systematic approach to determine the best software measurement setting for a given combination of material and inoculated concentration range of the test organism, resulting in a corresponding calibration curve.

The total concentration range spanned across 10^5 to $10^{8.5}$ cells/ml and was too wide to be captured within a single measurement setting, necessitating the division into two sub-ranges. These were designed to overlap in their intermediate concentrations and allowed the construction of continuous calibration curves where the detection ranges of both settings coincide. Two series of inoculations were performed, each consisting of nine algal concentrations with exponential steps of $10^{\circ.25}$ or $10^{\circ.5}$, covering a wide concentration range designed to capture the detection limits of the system and to account for the influence of substrate material on quantification reliability. The first concentration range covered concentrations from 10^5 to 10^7 cells/ml (low concentration range), while the second covered concentrations from 10^6 to $10^{8.5}$ cells/ml (high concentration range; Table 2).

Samples were prepared in quadruplicate, by inoculating 5 µL of algal suspension on the substrates for each concentration (see Section 2.4) and were measured with several different settings varying in ML and G (Fig. 2).

2.7. Selection of optimal software measurement settings and algal cell density-F_0 correlation

The calibration experiment was evaluated using a dedicated algorithm designed to identify the most reliable settings for calibration curve construction and to assess data quality in an unbiased and reproducible way. This algorithm was written in the Python programming language (Python 3.10.14, Python Software Foundation, Wilmington, Delaware, United States) using the development environment PyCharm (PyCharm, 2022.1 Community Edition, JetBrains, Czech Republic). Different libraries were implemented in the code. The library tkinter (Lundh, 1999) was used for GUI development, combined with openpyxl (Hunt, 2019) for handling Excel files. Pandas (Mckinney, 2010) and numpy (Harris et al., 2020) were implemented for data processing and statsmodels (Seabold and Perktold, 2010) for statistical analysis. Matplotlib (Hunter, 2007) allowed an initial data visualisation within the algorithm.

The algorithm contains validation criteria that ensure its applicability and the reliability of the calibration curve for algal concentrations compatible with early colonisation stage, while granting different levels of customisability. The validation criteria include (i) the assumption of a linear correlation between algal concentration and chlorophyll fluorescence signal; (ii) data consistency across all four replicates; (iii) the number of data points used for linear regression; (iv) reliability of the linear regression results.

Table 2
Inoculation concentrations.

Low algal inoculation concentration range		High algal inoculation concentration range	
Concentration of the algal suspension [cells/ml]	Number of algal cells on the substrate [algal cells/AOI]	Concentration of the algal suspension [cells/ml]	Number of algal cells on the substrate [algal cells/AOI]
$10^{5.00}$	$5.00 \cdot 10^2$	$10^{6.00}$	$5.00 \cdot 10^3$
$10^{5.25}$	$8.89 \cdot 10^2$	$10^{6.25}$	$8.89 \cdot 10^3$
$10^{5.50}$	$1.58 \cdot 10^3$	$10^{6.50}$	$1.58 \cdot 10^4$
$10^{5.75}$	$2.81 \cdot 10^3$	$10^{6.75}$	$2.81 \cdot 10^4$
$10^{6.00}$	$5.00 \cdot 10^3$	$10^{7.00}$	$5.00 \cdot 10^4$
$10^{6.25}$	$8.89 \cdot 10^3$	$10^{7.25}$	$8.89 \cdot 10^4$
$10^{6.50}$	$1.58 \cdot 10^4$	$10^{7.50}$	$1.58 \cdot 10^5$
$10^{6.75}$	$2.81 \cdot 10^4$	$10^{8.00}$	$2.81 \cdot 10^5$
$10^{7.00}$	$5.00 \cdot 10^4$	$10^{8.50}$	$1.58 \cdot 10^6$

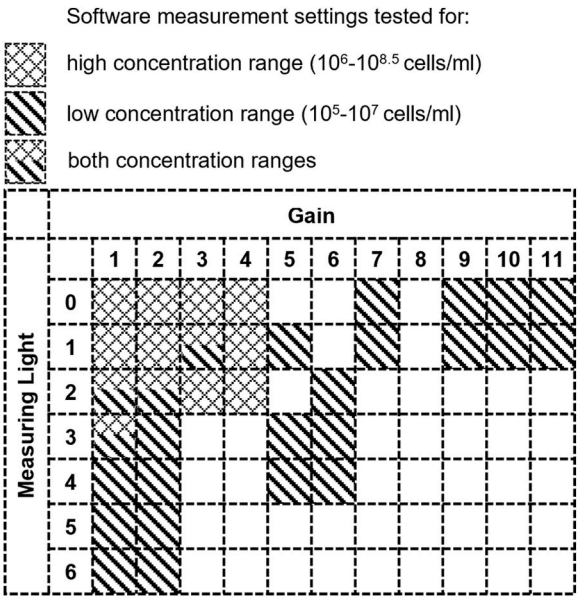

Fig. 2. Software measurement settings ML and G systematically tested on the materials with two concentration ranges. Hatched squares indicate the low concentration range; striped squares indicate the high concentration range (see Table 2 for details on concentration ranges). The low concentration range has been tested with low ML and high G, high ML and low G, or intermediate ML and G to highlight the algal presence. The high concentration range has been tested only for low ML and G because the highly concentrated algal inoculations easily saturated the signal. Some settings have been tested for both concentration ranges (squared half-hatched and half-striped).

3. Results

3.1. Material properties

Distinct differences were observed among the polycarbonate membranes, concrete pellets, and marble pellets. The corresponding material properties are summarised in Table 3, while detailed datasets for pH development over time and reflectance spectra are presented in Appendix (S3 and S4, respectively).

3.2. Algal viability assessment

Differences in chlorophyll fluorescence signal intensity and variability were observed among the substrate materials.

The compatibility between the substrates and *Jaagichlorella* sp. was confirmed in all cases, as the primary criterion for algal cell density, the F_0 signal intensity, remained sufficiently stable over the time of 8 h for both tested concentrations (Fig. 3, upper row). On polycarbonate

Table 3
Material properties.

	Polycarbonate membranes	Concrete pellets	Marble pellets
Reflectance [%R] (400-500 nm)	21.1 ± 0.6	16.1 ± 0.4	32.4 ± 0.2
L*	51.0	48.6	63.6
a*	−0.7	0.3	−0.4
b*	−3.3	2.5	−0.2
Opacity [contrast ratio]	76.35	x	x
Water contact angle [°]	97.5 ± 2.2	x	x
Porosity	0.2 µm[a]	7.5 %	7.8 %
pH after 24h	6.6 ± 0.2	7.9 ± 0.1	7.4 ± 0.2

[a] as from the producer.

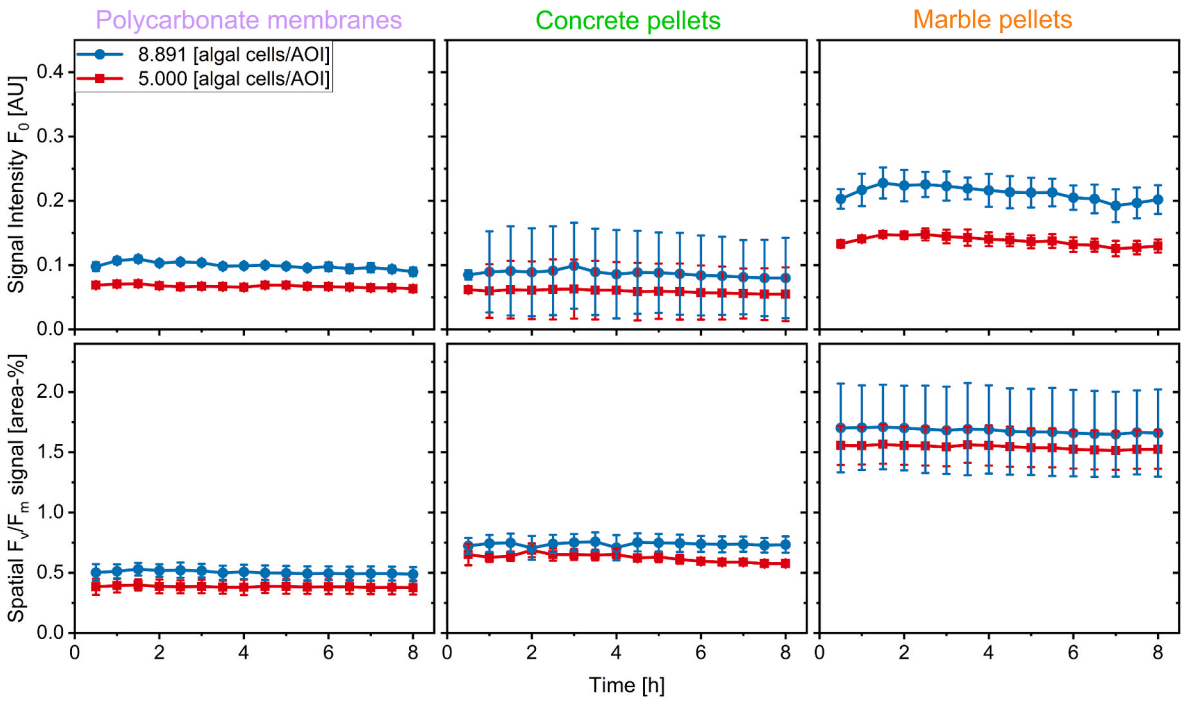

Fig. 3. Compatibility of *Jaagichlorella* sp. with the substrates over a 3-h contact period. The temporal development of F_0 signal intensity (top row) and F_v/F_m area-% coverage (bottom row) has been analysed over time with two algal concentrations. Across all materials, a direct effect of the substrate on the measured values is visible. Over the 8 h measurement period, the fluorescence data remained stable: at lower algal concentrations (red line with squares) the signals are consistent, while at higher inoculation levels (blue line with circles) they remain stable but with greater variance on concrete and marble pellets. (For interpretation of the references to colour in this figure legend, the reader is referred to the Web version of this article.)

membranes, both inoculated algal concentrations remained stable throughout the experiment, whereas measurements on concrete and marble pellets exhibited larger variability.

Spatial analyses showed that the area covered by the F_v/F_m signal and considered for F_0 signal intensity calculations remained constant throughout the 8-h measurement period, as indicated by the area-% values (Fig. 3, lower row).

The F_v/F_m signal intensity increased during the initial 1.5 h of measurement before reaching a stable level (Appendix, Fig. S5). This pattern was observed for both tested concentrations and across all three substrate materials.

3.3. Algorithm logic for systematic data evaluation

The algorithm provides a standardised and reproducible way to analyse the data obtained in a calibration experiment (see Section 2.6), automatically selecting optimal software measurement settings based on user-defined variables and leveraging the corresponding F_0 signal as a proxy for algal cell density to generate calibration curves. The algorithm relies on a structured spreadsheet (see Section on Code availability) and implements strict evaluation steps (Fig. 4, diamond shapes). A linear correlation between F_0 signal intensity and algal cell density, as commonly applied in similar calibrations (Eggert et al., 2006; Manso et al., 2014; Stock et al., 2019), was used to verify the data quality of each replicate. This assumption is proved false for algal inoculation concentrations beyond the lower or the upper detection limits, where the system becomes respectively undersaturated or oversaturated, and different concentrations either produce no detectable F_0 signal or result in F_0 signal intensities that do not correlate linearly with increasing algal cell density.

Linear fit quality is used for identifying detection limits. Due to commonly implemented exponential spacing within concentration ranges, the lower algal concentrations within a concentration range are always grouped closely at the beginning of that range, while the higher algal concentrations of the same range are more widely spaced (Table 2). This distribution of datapoints influences the effectiveness of linear regression, particularly at the lower ends, where subtle signal variations may not be readily captured. Therefore, an additional filtering strategy is implemented early in the data evaluation algorithm.

The algorithm logic (reported in Fig. 4) explicates all the steps of the software measurement settings selection, including the individual filtering of each replicate. As a first step, the inoculated algal concentrations and their corresponding signal intensities, sorted from lowest to highest inoculated algal concentration, are filtered. Within each replicate the current F_0 signal ($F_{0\ current}$) intensity is compared to the previous one. If the F_0 signal intensity passes the signal increase filter (S_i x $F_{0\ previous}$), it is categorised as valid and remains in the dataset. If the signal increase threshold is not met and the value is within the low end of the concentration range (Start), all preceding values are omitted. If an invalid value occurs within the upper end of the concentration range (End), it is omitted along with all subsequent datapoints.

The filtered data is then used to assess the consistency between replicates. For each inoculated algal concentration, the F_0 signal intensities are only kept if the required number of replicates contain a valid value, otherwise they are omitted. The remaining F_0 signal intensities of the replicates are averaged for each inoculated algal concentration, and standard deviation (SD) as well as the standard error of the mean (SEM) are calculated. This results in one dataset per unique combination of substrate material, software measurement setting and concentration range, containing only reliable measurement data.

Using these combined datasets, weighted linear regressions are performed. For each dataset, multiple linear fits are realised with a sliding window approach. The number of consecutive valid datapoints (n) used for linear regression must be at least a minimum value (n_{min}) and can extend up to the maximum number of datapoints (n_{max}) within the concentration range. To select the best linear regression for a data-

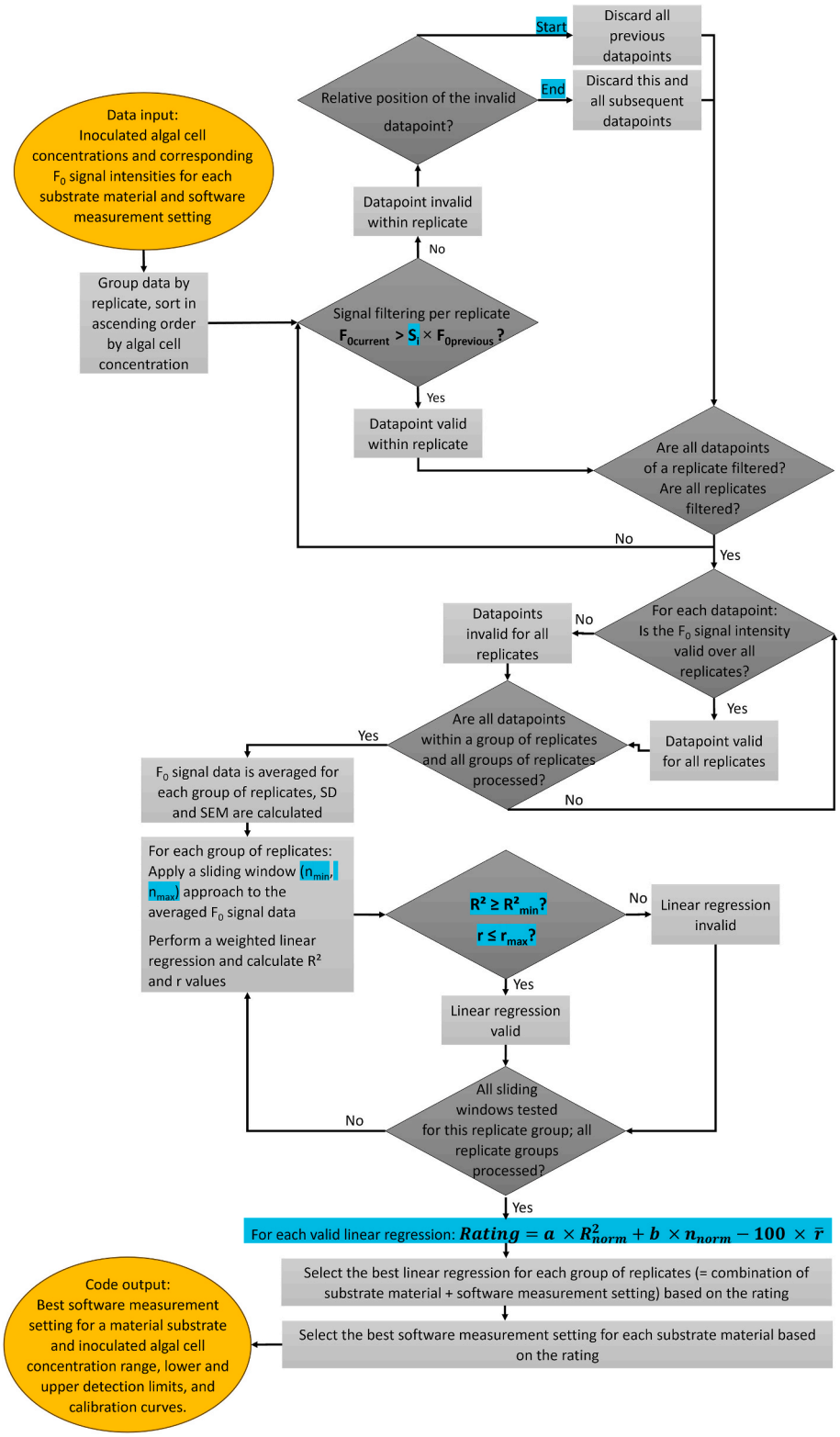

Fig. 4. Flow chart visualizing the functionality of the data processing algorithm. Ellipses represent inputs and outputs, diamonds indicate decision points, and rectangles denote processing steps. The algorithm begins with data import, followed by filtering of invalid measurements outside the detection range for each replicate. Replicates are then merged, retaining only valid data points present across all replicates. A sliding window linear regression is applied, and through a combination of filtering and rating-based evaluation, the optimal regression and software measurement settings are identified. Adaptable components of the algorithm are highlighted in blue areas, allowing for customization. (For interpretation of the references to colour in this figure legend, the reader is referred to the Web version of this article.)

set, the goodness of fit (R^2) and the residuals (r) as a measure between observed (y_i) and calculated value ($\hat{y}_i$) are computed. Linear regressions containing r values higher than a set maximum or a R^2 value below a set minimum (R^2_{min}) are omitted (Fig. 4).

$$R^2_{norm} = \frac{(R^2 - R^2_{min})}{(R^2_{max} - R^2_{min})} \quad [2]$$

$$n_{norm} = \frac{(n - n_{min})}{(n_{max} - n_{min})} \quad [3]$$

$$r = y - \hat{y} \quad [4]$$

$$\bar{r} = \frac{1}{n}\sum_{i=1}^{n} |y_i - \hat{y}_i| \quad [5]$$

$$Rating = a \times R^2_{norm} + b \times n_{norm} - 100 \times \bar{r} \quad [6]$$

The remaining linear regressions are subjected to a rating procedure, selecting only one linear fit per dataset. The final rating takes into account the normalised R^2 (R^2_{norm}), the normalised amount of datapoints used for this linear regression (n_{norm}) and the absolute mean residual ($\bar{r}$) as well as adjustable weighting parameters (a, b), resulting in the most suitable software measurement setting and the best fitting linear regression.

3.4. Selected software measurement settings and linear regressions

The data evaluation algorithm containing the validation criteria (see Section 2.7) was implemented with the variables that can be tailored to the specific boundary conditions of the calibration experiment (see Section 3.3).

In our case, the validation criteria were met with a minimum of four consecutive, valid datapoints (Table 4, Sliding window variable). The remaining data was rated with a balanced fit between goodness of fit and calibration range width (Table 4), and the most suitable dataset was selected.

Using the algorithm, different software measurement settings were selected for the tested scenarios. ML was always between 0 and 1, while G correction ranged between 1 and 10 (Table 5), with significant differences between substrates and concentration ranges. All calibration curves showed a linear fit with R^2 values always higher than 0.986. The lowest R^2 value was reported for marble pellets combined with the high algal inoculation concentration range.

The output of the data evaluation algorithm (Table 5) can be cross-referenced to the original, visual ImagingWin data (Fig. 5). Inoculated areas showed a concentric layering of signal intensities, with the highest chlorophyll fluorescence values in the centre, surrounded by concentric rings of decreasing intensities. This effect was more pronounced for higher inoculation concentrations in each range, which coincided with visually larger fluorescence area diameter (Fig. 5, C1). At lower inoculated algal concentrations within each range, all three substrates exhibited unevenly distributed chlorophyll fluorescence, with only a small area detected in the middle of the AOI (Fig. 5, A1, B1, C1).

Inoculated algal suspensions on polycarbonate membranes (Fig. 5, A1 - A4) and concrete pellets (Fig. 5, B1 - B4) visually showed smaller fluorescent areas for both F_0 and F_v/F_m compared to inoculations on marble pellets, and were slightly larger on concrete pellets than on polycarbonate membranes. Both substrates showed little concentric layering.

In direct comparison, marble pellets displayed higher F_0 signals for lower algal inoculated concentrations, but when progressing from intermediate to high algal inoculated concentrations, fluorescent area diameter and concentric layering increased (Fig. 5, C1, C3). These effects were more evident in the F_v/F_m view, where the higher inoculation concentrations resulted in F_v/F_m signal intensities of 0, visualized as AOIs with black centres (Fig. 5, C2, C4). Consequently, the F_0 view does not reliably display oversaturation (Fig. 5, C1, C3) and the effect is more apparent in the F_v/F_m view (Fig. 5, C2, C4). However, when focusing on a particularly high datapoint (Fig. 5 C3 and C4, Point 9) visual assessment alone did not indicate a measurement error.

Table 4
Algorithm parameters.

Variable	Type	Abbreviation	Value
Signal threshold increase	Filter	S_i	5 %
Initial Concentration span	Range span	Start	1 – 4
Terminal Concentration span	Range span	End	5 – 9
Sliding window minimum	Minimum number of reliable, subsequent data points	n_{min}	4
Sliding window maximum	Maximum number of reliable, subsequent data points	n_{max}	9
Maximum residual	Filter	r_{max}	20 %
Minimum R^2	Filter	R^2_{min}	0.8
Rating parameter	Weighting parameter	a	0.5
Rating parameter	Weighting parameter	b	0.5

3.5. Calibration curve for Jaagichlorella sp. on different substrate materials

Calibration curves for all tested materials were established by correlating the F_0 signal intensities with defined concentrations of inoculated *Jaagichlorella* sp. suspensions (Fig. 6). The section of the data that exhibits a linear relationship was determined by the data evaluation algorithm, as detailed in Section 3.3.

The slopes of the calibration curves (Table 5, Fig. 6B), as well as the comprehensive calibration curve including both concentration ranges differed between substrates (Fig. 6). The higher and lower calibration ranges partially overlapped for the polycarbonate membranes between 10^6 cells/ml and $10^{6.5}$ cells/ml, and for marble pellets for 10^6 cell/ml (concentration conversions in Table 2). For these two materials, this overlap allowed the construction of an extended, continuous calibration curve covering a concentration range from $10^{5.5}$ to 10^7 cells/ml (Fig. 6B). Concrete pellets exhibited a complete overlapping of the calibration range for the higher and the lower algal concentrations, resulting in a calibration curve covering from 10^6 to 10^7 cells/ml (Fig. 6B).

Polycarbonate membranes and concrete pellets showed similar trends in their curvilinear graphs, both displaying a plateau for the highest concentrations and F_0 signals. Moreover, they shared the selected software measurement setting for the low algal concentration range, whereas concrete pellets required a higher G correction to amplify the signal for the higher concentration range. In comparison, marble pellets required the same ML, but a higher G to amplify the F_0 signal for the lower concentration range (Fig. 6A). For the higher concentration range, marble pellets required lower ML among every measured set (ML 0), combined with a low G correction.

As a general trend, marble pellets showed higher absolute F_0 signal intensities with respect to polycarbonate membranes and concrete pellets for the same concentrations. Moreover, after surpassing the detectability limit, the F_0 signal intensity decreased without forming a plateau, with particularly increased SDs for the lower concentration range (Fig. 6A). Regarding the higher concentration range, the decrease in F_0 signal intensity is followed by a subsequent increase of this parameter (Fig. 6A). These differences in material performance are qualitatively observable by visual imaging, as oversaturation on marble pellets appeared different from the other materials for both concentration ranges (Fig. 5, C1 – C4).

Table 5
Selected settings.

Tested Scenarios		Outputs of the data processing algorithm				ImagingWin View	
Material substrate	Concentration range [cells/ml]	Software measurement setting	Linear Regression	R^2	Calibration range [cells/ml]	F_0	F_v/F_m
Polycarbonate membranes	$10^{5.00} - 10^{7.00}$	ML 1 G 9	5.77E-06 · x + 0.027	0.993	$10^{5.50} - 10^{6.50}$	A1	A2
Polycarbonate membranes	$10^{6.00} - 10^{8.50}$	ML 1 G 2	1.97E-06 · x + 0.021	0.998	$10^{6.00} - 10^{7.00}$	A3	A4
Concrete pellets	$10^{5.00} - 10^{7.00}$	ML 1 G 9	3.61E-06· x + 0.022	0.999	$10^{6.00} - 10^{6.75}$	B1	B2
Concrete pellets	$10^{6.00} - 10^{8.50}$	ML 1 G 4	1.86E-06 · x + 0.016	0.997	$10^{6.00} - 10^{7.00}$	B3	B4
Marble pellets	$10^{5.00} - 10^{7.00}$	ML 1 G 10	1.81E-05 · x + 0.024	0.998	$10^{5.50} - 10^{6.25}$	C1	C2
Marble pellets	$10^{6.00} - 10^{8.50}$	ML 0 G 1	4.04E-06 · x + 0.038	0.986	$10^{6.25} - 10^{7.00}$	C3	C4

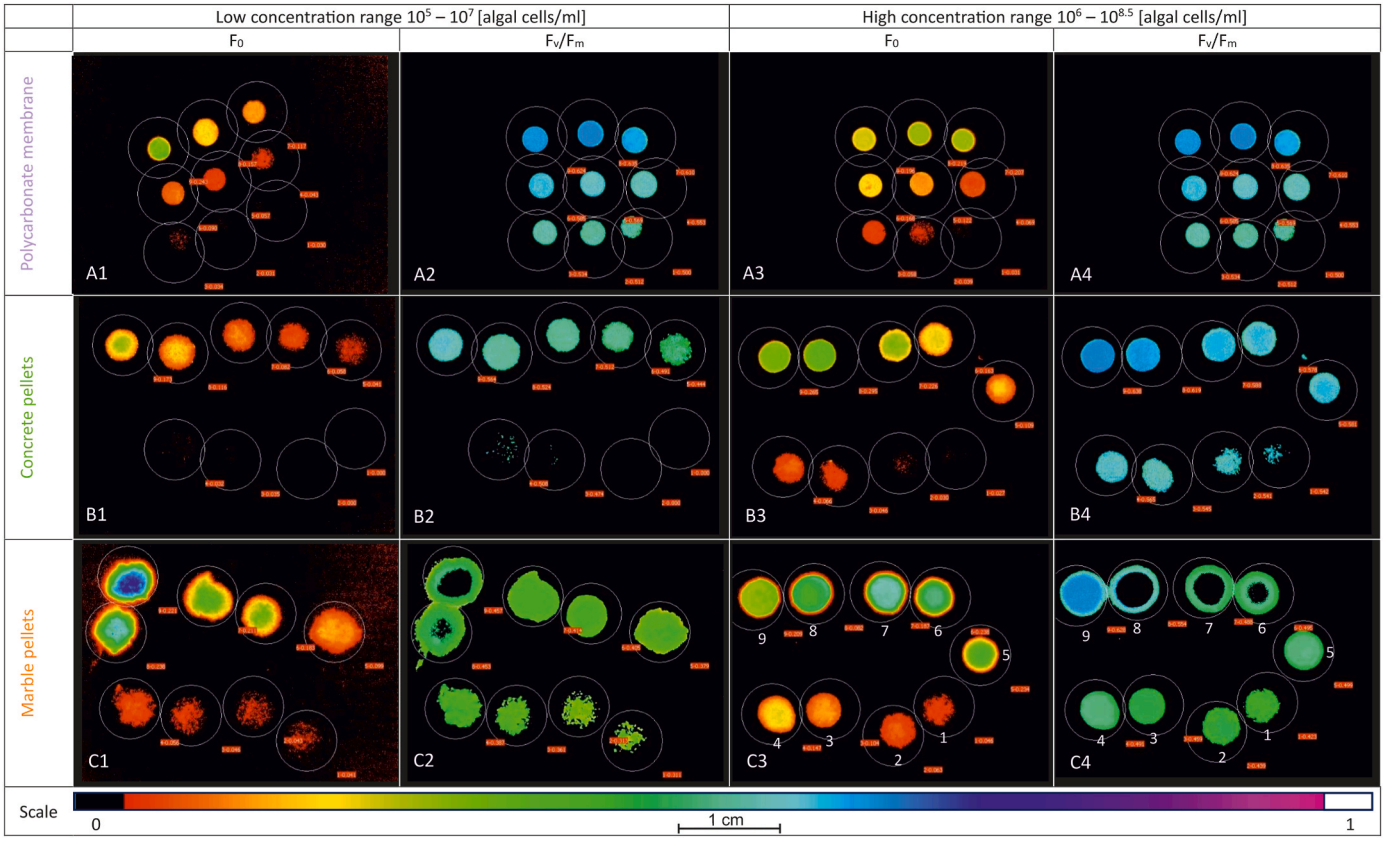

Fig. 5. Visual data collected with the optimal software measurement settings selected by the data processing algorithm. For each tested scenario, F_0 and F_v/F_m images of one replicate are shown. Algal concentrations are always within the defined AOI (white circles), and the fluorescence data extracted is depicted adjacent to each AOI (red box). Undersaturation effects are visible in the F_0 signal intensity images (A1, A3, B1, B3), where the lowest concentrations are barely detectable. In contrast, oversaturation effects are visible on marble pellets as strong concentric layering (C1, C3) and corresponding signal errors in the F_v/F_m view (C2, C4). Panels C3 and C4 are additionally labelled with numbers 1–9, representing increasing inoculated algal concentrations from the lowest (1) to the highest (9). Notably, the highest concentration (9), despite being recognised as faulty by the data processing algorithm (Paragraph 3.4), appears visually acceptable. (For interpretation of the references to colour in this figure legend, the reader is referred to the Web version of this article.)

4. Discussion

This study offers a practical framework for Imaging PAM-F calibration, with a specific focus on detecting low algal densities under controlled laboratory conditions. A highly standardised sample preparation and data collection process were implemented. The F_0 signal of the subaerial green alga *Jaagichlorella* sp. inoculated on different materials was measured with systematically varied ML and G device software parameters.

An ad hoc, customisable evaluation algorithm for unbiased measurement setting selection and calibration curves elaboration was developed and successfully applied to our case study (see Section 4.1). The compatibility of the selected algal strain with the materials and the calibration procedure (see Section 4.2) as well as the impact of material properties on Imaging PAM-F signals (see Section 4.3) are also discussed.

4.1. Algorithm customisability and use for bioreceptivity studies

Imaging PAM-F devices allow a visual evaluation of many fluorescence parameters, including the F_0-value correlated to algal cell density. However, tuning software parameters often relies on trial-and-error. This non-standardised use, together with the lack of reporting selected software parameters, reduces reproducibility. Moreover, selecting optimal software settings based solely on visual cues requires considerable user experience, and introduces a risk of error.

As a practical example, the F_0 signals for marble pellets inoculated with high concentrations seem within detectability range when

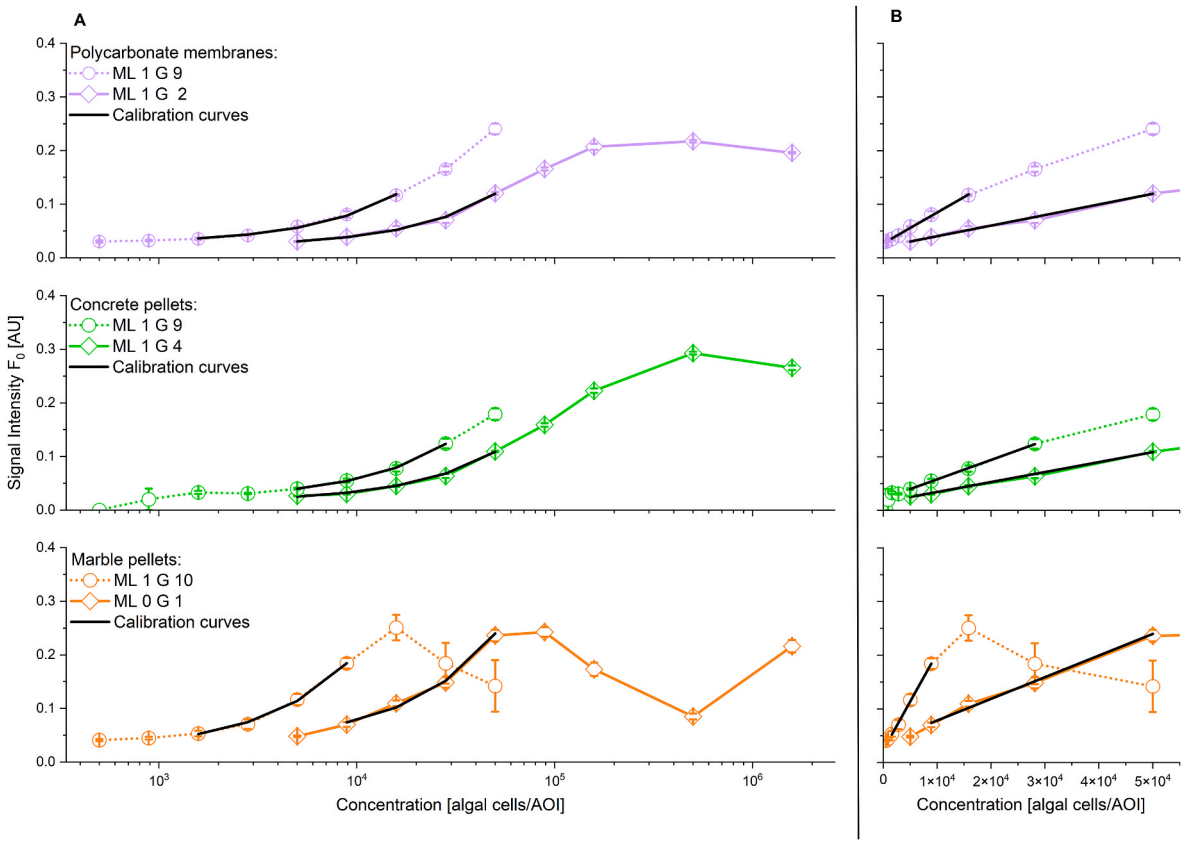

Fig. 6. Calibration curves for *Jaagichlorella* sp. on different substrate based on the selected optimal measurement settings. The low concentration range (dotted line) and the high concentration range (continuous line) overlap for polycarbonate membranes (purple lines), concrete pellets (green lines) and marble pellets (orange lines). Calibration curves were established for all tested scenarios (black lines). A: Correlation between F_0 signal and algal cell density on a logarithmic scale over the full range of tested concentrations. The curves exhibit a curvilinear shape. Plateaus in the beginning of the concentration range are due to undersaturation, as insufficient chlorophyll fluorescence from the inoculated alga prevents reliable quantification. Terminal plateaus, which are especially pronounced and unpredictable in marble pellets, are due to oversaturation and beyond the upper detection limit. Calibration curves were created using the linear part of the curve. B: Correlation between F_0 signal and algal cell density on a linear scale, with focus on the calibration curves. Calibration curves cover different ranges and exhibit different slopes due to different software measurement setting or material properties. (For interpretation of the references to colour in this figure legend, the reader is referred to the Web version of this article.)

evaluated visually (Fig. 5-C1); yet the corresponding F_v/F_m signal (Fig. 5-C2) reveals oversaturation effects. Moreover, fluorescence signals exceeding the upper detection limit may not cause an obvious plateau in signal intensity but instead result in lower signals recorded. This effect, visible in Fig. 6 for high concentrations on marble pellets, is likely due the "primary and secondary inner filter", an effect of partial absorption and scattering of excitation light widely known for fluorophores (Schagerl et al., 2022). Such errors may lead to severe underestimation of algal cell density when assessed without the context of a larger concentration range.

Our algorithm for software setting selection and calibration curve generation addresses and solves these problems caused by lack of standardisation. Based on the input of inoculated algal concentrations and corresponding measured F_0-values using different combinations of ML and G, the algorithm identifies optimal software measurement settings and generates reliable calibration curves (Fig. 4, Table 5). The algorithm presents a high degree of customisability. Filtering variables and weighting parameters (Table 4) are easily adjustable, making the algorithm highly adaptable to a wide range of experimental designs. The final selection is made with a rating equation (Eq. (6)), whose parameters offer the flexibility of prioritising either linear fit quality or calibration range. The results are presented in a user-friendly and fully transparent format which can be easily transferred (Table 5).

However, linearity may be compromised in cases such as measuring cyanobacteria and red algae with PAM-F devices equipped with blue light, due to different and pigment-specific excitation (Gustavs et al., 2009). Consequently, the suitability of the PAM-F device and its excitation light for different photosynthetic organisms must be considered.

The linear correlation is also lost at higher cell densities, as increased layering of algal cells creates a shading effect (Manso et al., 2014; Stock et al., 2019) and results in an underestimation (Schmitt-Jansen and Altenburger, 2008). This limitation for mature biofilms does not impact studies focused on initial colonisation which require quantification of subtle changes in algal cell density.

The complementary visual assessment of the spatial information provided by Imaging PAM-F remains a key advantage of this technique and is recommended when evaluating the application of the protocol to new test organisms, materials or devices to capture the qualitative changes in the F_0 signal. However, by implementing the customisable ad hoc algorithm, the visual and user-dependent evaluation is just the first step and complimented by a transparent, data-driven process. The algorithm proposed enables users with limited Imaging PAM-F experience to generate calibration curves for defined algal concentration ranges, making this method accessible for a broader, interdisciplinary field of application.

4.2. Jaagichlorella sp. as a reference strain for imaging PAM-F calibrations and bioreceptivity studies

In our experiment, *Jaagichlorella* sp. was cultured and harvested

under highly controlled conditions (see Section 2.2) and the quantification was performed via manual cell counting. This technique is time-consuming, making it unsuitable for frequent monitoring (Schagerl et al., 2022), and it cannot be used for filamentous algae (Gustavs et al., 2009). Nevertheless, in the context of this study it was the most suitable direct quantification method, due to its high precision and reliability for microalgae (Lund et al., 1958; Proença et al., 2022).

Moreover, the compatibility of *Jaagichlorella* sp. with all three substrates was confirmed. As shown in Fig. 3, the stability of the F_0 signal intensities and the F_v/F_m signal area over the measurement period of 8 h highlights this strain as a reliable test microorganism for establishing calibration curves of coccoid green algae on different materials.

The initial increase in F_v/F_m signal intensities within the first 1.5 h (Appendix S5) was likely caused by hydric stress associated with the inoculation procedure, as water stress is known to affect PAM-F signals (Romeu et al., 2020; Fuentes Alonso and Prieto, 2021b).

The high variability observed on concrete pellets, together with the calibration results (see Section 3.5), suggests that the combination of substrate and algal cell density approached the lower sensitivity limit, particularly at the lower inoculation concentration. However, cementitious materials are known for their high pH values (Thu Hien et al., 2012; Dalod et al., 2014; Manso et al., 2014; Grosseau et al., 2015), and a potential inhibitory effect must be accounted for. The pH measurements (see Section 3.1) revealed while the concrete pellets show the highest pH value of the substrates, their pH still remains below 8., suggesting that the pH value of the selected materials did not have a significant effect. Paired with the observed stability of the F_v/F_m value (Fig. 3, Appendix S5), this confirms *Jaagichlorella* sp. tolerance to the measured pH range between 6.6 and 7.9.

No relevant influence on the F_0 signal intensity was observed over the course of a few hours, confirming *Jaagichlorella* sp. as a reliable test organism, suitable for future bioreceptivity studies with Imaging PAM-F techniques.

4.3. Substrate impact on imaging PAM-F measurements

The concentric layering of the fluorescence signal intensities (see Section 3.4) was previously described by Eggert and colleagues (2006) over the whole measurement area, and attributed to the lighting system of Imaging PAM-F devices. Instead, in our study the concentric layering was visible not per measurement image, but for every droplet independently. Moreover, the intensity of the concentric layering differed among substrates, suggesting that this effect was substrate-specific rather than a device artefact. Together with the observed differences in chlorophyll fluorescence signal intensity and area (Fig. 3, Appendix S5), these findings demonstrate a strong influence of material properties on Imaging PAM-F measurements.

The selected substrates showed different reflectance in the wavelength-range relevant for our Imaging PAM-F device (Table 3, Appendix S3). Marble pellets as the lightest and most reflective substrate showed the highest droplet area coverage, concentric layering, and reached oversaturation most easily. Concrete was on the other side of the spectrum, with the lowest reflectance and darkest surface, combined with being particularly prone to undersaturation. Polycarbonate membranes represent an intermediate case, which is in accordance with their behaviour during measurements; and their reduced opacity did not seem to have an influence. These results suggest that substrate reflectance and colour significantly influence signal intensities and, consequently the visual appearance of Imaging PAM-F measurements.

However, measurements of the fluorescence signal also depend on the spreading of the algal inoculate on a materials surface, which is influenced by impact velocity, inoculate viscosity, and material porosity (Basit et al., 2018). The presented protocol relied on a consistent inoculation method and assumed inoculate viscosity (the latter likely depending on algal concentration), suggesting that material porosity and wettability are the decisive factors influencing Imaging PAM-F measurements.

Substrate porosity must allow moisture retention without dragging and shading algal cells inside the pores (von Werder and Venzmer, 2013) to ensure accurate quantification. The porosity of the mineral pellets was similar to each other but differed from that of the polycarbonate membrane. However, no clear relationship was observed between the measured porosity values and either droplet spreading or chlorophyll fluorescence signal.

Differences in wettability were observed among all three substrates. Polycarbonate membranes were the only substrates that maintained a measurable water contact angle (Table 3), which corresponded to a relatively small droplet coverage area (Fig. 5). Droplet areas were slightly larger on concrete pellets, which exhibited optical properties similar to those of the polycarbonate membranes but showed no measurable water contact angle, indicating higher wettability. In contrast, droplet areas were substantially larger on marble pellets. While this may partly be attributable to differences in optical properties, droplets on marble pellets were also prone to deformation (Fig. 5), suggesting the influence of an additional factor. Although the two mineral substrates exhibited similar overall porosity, differences in macroscopic pore size distribution may affect wettability (Meng et al., 2014), and could therefore explain the observed droplet deformation.

Taken together, these substrate properties led to marble pellets consistently producing higher signals (Fig. 5) than concrete pellets and polycarbonate membranes (Fig. 5). As a result, polycarbonate membranes and concrete pellets required stronger ML and/or G correction for amplifying the F_0 signal, particularly at low algal cell densities (Table 5). Differences in signal intensity among the tested substrates determined both the optimal software measurement settings and the concentration ranges over which reliable calibration curves could be established. Owing to its high sensitivity, Imaging PAM-F can detect very low algal cell densities and resolve the earliest stages of biofilm formation (Schreiber, 2004; Eggert et al., 2006; von Werder and Venzmer, 2013), which are often not covered by conventional analytical tools. In our case study, the resulting calibration curves covered low algal cell density ranges fully compatible with initial colonisation phases. The division in two separate concentration ranges (see Section 2.6) was chosen to accommodate photosynthetic biofilm development over time in long term bioreceptivity studies. Indeed, the initial inoculation concentration can be strategically selected within the lower calibration range, allowing biofilm development to be monitored over the widest possible range. Biofilm development can be tracked along the calibration curve and transition to the measurement setting of the higher calibration range when approaching the overlap zone between ranges. Additionally, the oversized AOI also allow monitoring of spatial algal growth. While validation of this dynamic monitoring approach requires further investigation, this design enables material bioreceptivity to be assessed quantitatively and consistently across laboratories. The standardized framework provides reliable and customisable measurements that account for both algal stress tolerance and the specific properties of the substrate material.

5. Conclusion

We presented the first standardised, data-driven Imaging PAM-F method for quantitative bioreceptivity assessment on different materials. The calibrated workflow accurately detected low algal cell densities present during early biofilm development and produced linear calibration curves between *Jaagichlorella* sp. cell density and F_0 signals on concrete and marble pellets, as well as on polycarbonate membranes. Data were assessed through an objective evaluation algorithm, which greatly improves experimental reproducibility, particularly related to the selection of software measurement settings, and enables comparability across Imaging PAM-F datasets.

The results confirm that material properties, specifically reflectance, directly influence chlorophyll fluorescence signals measured by Imaging

PAM-F. Distinct sensitivity limits were identified for each material: concrete pellets and polycarbonate membranes were prone to undersaturation at low algal cell densities, whereas marble pellets readily approached oversaturation at higher cell densities. These findings show that measurement settings and calibration curves are substrate-specific and cannot be directly transferred from one material to another, even when the same algal strain is used.

Despite these substrate-dependent effects, *Jaagichlorella* sp. proved to be a robust and ecologically relevant test organism for bioreceptivity testing. F_0 and F_v/F_m measurements remained stable over the extended calibration period, indicating compatibility with all tested substrates and confirming the suitability of the strain for prolonged Imaging PAM-F measurements.

CRediT authorship contribution statement

Leonie Stohl: Writing – review & editing, Writing – original draft, Visualization, Software, Methodology, Investigation, Formal analysis, Conceptualization. **Jake Cook:** Writing – review & editing, Methodology, Investigation, Conceptualization. **Julia von Werder:** Writing – review & editing, Resources, Project administration, Funding acquisition, Conceptualization. **Anna A. Gorbushina:** Writing – review & editing, Visualization, Resources, Conceptualization. **Chiara Tonon:** Writing – review & editing, Writing – original draft, Supervision, Software, Methodology, Investigation, Conceptualization.

Code availability

The data evaluation algorithm written in Python will be made available as open-source software in a GitHub Repository. Both the structure spreadsheet and the data evaluation algorithm will be made available under the DOI 10.5281/zenodo.17184039.

Declaration of generative AI and AI-assisted technologies in the writing process

During the preparation of this work the author(s) used CoPilot for in order to improve clarity, grammar and overall readability. After using these tools, the author(s) reviewed and edited the content as needed and take(s) full responsibility for the content of the published article.

Declaration of competing interest

The authors declare that they have no known competing financial interests or personal relationships that could have appeared to influence the work reported in this paper.

Acknowledgements

This study was supported by the Bundesministerium für Wohnen, Stadtentwicklung und Bauwesen (Award Number: 10.08.18.7-21.07 AbifFa), the Bundesanstalt für Materialforschung und -prüfung (Award Number: MI1462), which also provided internal funding.

The authors would like to thank Elsa Fuentes Alonso for insightful discussions and André Gardei for technical support.

Appendix A. Supplementary data

Supplementary data to this article can be found online at https://doi.org/10.1016/j.ibiod.2026.106455 (https://doi.org/10.5281/zenodo.17184038).

Data availability

The experimental data obtained with Imaging PAM-F will be made available under the https://doi.org/10.5281/zenodo.17184214.

References

Baishya, R., 2024. Application of FESEM and FTIR for evaluation of *Staphylococcus aureus* biofilms grown on chitin and polycarbonate membrane. Rev. Mex. Ing. Quim. https://doi.org/10.24275/RMIQ/MAT2175.

Baker, N.R., 2008. Chlorophyll fluorescence: a probe of photosynthesis in vivo. Annu. Rev. Plant Biol. 59, 89–113. https://doi.org/10.1146/annurev.arplant.59.032607.092759.

Basit, A., KuShaari, K., Siwayanan, P., Azeem, B., 2018. Effect of process parameters on droplet spreading behaviour over porous surface. Can. J. Chem. Eng. 96, 352–359. https://doi.org/10.1002/cjce.22925.

Cappitelli, F., Cattò, C., Villa, F., 2020. The control of cultural heritage microbial deterioration. Microorganisms 8, 1542. https://doi.org/10.3390/microorganisms8101542.

Carpentier, C., Dahlhaus, A., Giesen, N. van de, Maršálek, B., 2013. The influence of hard substratum reflection and calibration profiles on in situ fluorescence measurements of benthic microalgal biomass. Environ. Sci. Process. Impacts 15, 783–793. https://doi.org/10.1039/C3EM30654B.

Castle, S.C., Morrison, C.D., Barger, N.N., 2011. Extraction of chlorophyll a from biological soil crusts: a comparison of solvents for spectrophotometric determination. Soil Biol. Biochem. 43, 853–856. https://doi.org/10.1016/j.soilbio.2010.11.025.

Cheng, F., 2013. Using building codes and standards to improve construction quality and safety. In: ICCREM 2013, pp. 113–120. https://doi.org/10.1061/9780784413135.010.

Contreras, J.L., Roth, H., Lewis, M., 2011. Toward a rational framework for sustainable building materials standards. Environ. Law Pol. eJ. 63, 1–6.

Cutler, N.A., Viles, H.A., Ahmad, S., McCabe, S., Smith, B.J., 2013. Algal 'greening' and the conservation of stone heritage structures. Sci. Total Environ. 442, 152–164. https://doi.org/10.1016/j.scitotenv.2012.10.050.

Dalod, E., Govin, A., Guyonnet, R., Grosseau, P., Lors, C., Damidot, D., 2014. Influence of the chemical composition of mortars on algal biofouling. International Conference on Calcium Aluminates. IHS BRE Press, pp. 523–534.

De Muynck, W., Ramirez, A.M., De Belie, N., Verstraete, W., 2009. Evaluation of strategies to prevent algal fouling on white architectural and cellular concrete. Int. Biodeterior. Biodegrad. 63, 679–689. https://doi.org/10.1016/j.ibiod.2009.04.007.

Dökümcüoğlu, V.E., Yılmaz, M., 2020. Assessment of cell counting method based on image processing for a microalga culture. MedFAR 3, 75–81.

Eggert, A., Häubner, N., Klausch, S., Karsten, U., Schumann, R., 2006. Quantification of algal biofilms colonising building materials: chlorophyll a measured by PAM-fluorometry as a biomass parameter. Biofouling 22, 79–90. https://doi.org/10.1080/08927010600579090.

Elgaali, H.H., Lopez-Arias, M., Velay-Lizancos, M., 2024. Accelerated CO_2 exposure treatment to enhance bio-receptivity properties of mortars with natural and recycled concrete aggregate. Constr. Build. Mater. 449, 138423. https://doi.org/10.1016/j.conbuildmat.2024.138423.

Figueroa, F.L., Jerez, C.G., Korbee, N., 2013. Use of in vivo chlorophyll fluorescence to estimate photosynthetic activity and biomass productivity in microalgae grown in different culture systems. Latin Am. J. Aqua. Res. 41, 801–819. https://doi.org/10.3856/vol41-issue5-fulltext-1.

Fuentes Alonso, E., Prieto, B., 2021a. A laboratory approach on the combined effects of granite bioreceptivity and parameters modified by climate change on the development of subaerial biofilms on cultural heritage. Int. Biodeterior. Biodegrad. 164, 105295. https://doi.org/10.1016/j.ibiod.2021.105295.

Fuentes Alonso, E., Prieto, B., 2021b. Recovery capacity of subaerial biofilms grown on granite buildings subjected to simulated drought in a climate change context. Microb. Ecol. 82, 761–769. https://doi.org/10.1007/s00248-021-01692-0.

Genty, B., Briantais, J.-M., Baker, N.R., 1989. The relationship between the quantum yield of photosynthetic electron transport and quenching of chlorophyll fluorescence. Biochim. Biophys. Acta Gen. Subj. 990, 87–92. https://doi.org/10.1016/S0304-4165(89)80016-9.

Gladis, F., Schumann, R., 2011a. A suggested standardised method for testing photocatalytic inactivation of aeroterrestrial algal growth on TiO_2-coated glass. Int. Biodeterior. Biodegrad. 65, 415–422. https://doi.org/10.1016/j.ibiod.2011.01.005.

Gladis, F., Schumann, R., 2011b. Influence of material properties and photocatalysis on phototrophic growth in multi-year roof weathering. Int. Biodeterior. Biodegrad. 65, 36–44. https://doi.org/10.1016/j.ibiod.2010.05.014.

Gorbushina, A., 2007. Life on the rocks. Environ. Microbiol. 9, 1613–1631. https://doi.org/10.1111/j.1462-2920.2007.01301.x.

Grosseau, P., Dalod, E., Govin, A., Lors, C., Guyonnet, R., Damidot, D., 2015. Effect of the chemical composition of building materials on algal biofouling. Concrete 2015/RILEM week - 27th biennial national conference of the concrete institute of Australia in conjunction with the 69th RILEM week. Concrete Inst. Australia 735–à 744. emse-01206843f.

Guillitte, O., 1995. Bioreceptivity: a new concept for building ecology studies. Sci. Total Environ. 167, 215–220. https://doi.org/10.1016/0048-9697(95)04582-L.

Gustavs, L., Schumann, R., Eggert, A., Karsten, U., 2009. In vivo growth fluorometry: accuracy and limits of microalgal growth rate measurements in ecophysiological investigations. Aquat. Microb. Ecol. 55, 95–104. https://doi.org/10.3354/ame01291.

Harris, C.R., Millman, K.J., van der Walt, S.J., Gommers, R., Virtanen, P., Cournapeau, D., Wieser, E., Taylor, J., Berg, S., Smith, N.J., Kern, R., Picus, M., Hoyer, S., van Kerkwijk, M.H., Brett, M., Haldane, A., del Río, J.F., Wiebe, M., Peterson, P., Gérard-Marchant, P., Sheppard, K., Reddy, T., Weckesser, W., Abbasi, H., Gohlke, C., Oliphant, T.E., 2020. Array programming with NumPy. Nature 585, 357–362. https://doi.org/10.1038/s41586-020-2649-2.

Häubner, N., Schumann, R., Karsten, U., 2006. Aeroterrestrial microalgae growing in biofilms on facades—response to temperature and water stress. Microb. Ecol. 51, 285–293. https://doi.org/10.1007/s00248-006-9016-1.
Hunt, J., 2019. Working with excel files. In: Advanced Guide to Python 3 Programming. Undergraduate Topics in Computer Science. Springer, pp. 249–255. https://doi.org/10.1007/978-3-030-25943-3_21.
Hunter, J.D., 2007. Matplotlib: a 2D graphics environment. Comput. Sci. Eng. 9, 90–95. https://doi.org/10.1109/MCSE.2007.55.
Jakob, T., Schreiber, U., Kirchesch, V., Langner, U., Wilhelm, C., 2005. Estimation of chlorophyll content and daily primary production of the major algal groups by means of multiwavelength-excitation PAM chlorophyll fluorometry: performance and methodological limits. Photosynth. Res. 83, 343–361. https://doi.org/10.1007/s11120-005-1329-2.
Jakubovskis, R., 2024. Biophilic facades: the potentiality of bioreceptive concrete. Preprints 2024. https://doi.org/10.20944/preprints202411.0678.v1.
Karsten, U., Herburger, K., Holzinger, A., 2014. Dehydration, temperature and light tolerance in members of the aeroterrestrial green algal genus *Interfilum* (Streptophyta) from biogeographically different temperate soils. J. Phycol. 50. https://doi.org/10.1111/jpy.12210.
Karsten, U., Herburger, K., Holzinger, A., 2016. Photosynthetic plasticity in the green algal species *Klebsormidium flaccidum* (Streptophyta) from a terrestrial and a freshwater habitat. Phycologia 56 (1). https://doi.org/10.2216/16-85.
Karsten, U., Rindi, F., 2010. Ecophysiological performance of an urban strain of the aeroterrestrial green alga *Klebsormidium* sp. (Klebsormidiales, Klebsormidiophyceae). Eur. J. Phycol. 45, 426–435. https://doi.org/10.1080/09670262.2010.498587.
Kautsky, H., Hirsch, A., 1931. Neue Versuche zur Kohlensäureassimilation. Naturwissenschaften 19. https://doi.org/10.1007/BF01516164, 964–964.
Komar, M., Derese, N., Szymczak, K., Nowicka-Krawczyk, P., Gutarowska, B., 2025. Natural plant oils as anti-algae biocides for sustainable application in cultural heritage protection. Sustainability 17, 6996. https://doi.org/10.3390/su17156996.
Li, S., Fanesi, A., Martin, T., Lopes, F., 2024. Physiological transition of *Chlorella vulgaris* from planktonic to immobilized conditions. Algal Res. 77, 103354. https://doi.org/10.1016/j.algal.2023.103354.
Li, Y.H., Wang, D., Xu, X.T., Gao, X.X., Sun, X., Xu, N.J., 2017. Physiological responses of a green algae (*Ulva prolifera*) exposed to simulated acid rain and decreased salinity. Photosynthetica 55, 623–629. https://doi.org/10.1007/s11099-017-0689-0.
Lund, J., Kipling, C., Le Cren, E.D., 1958. The inverted microscope method of estimating algal numbers and the statistical basis of estimations by counting. Hydrobiologia 11, 143–170. https://doi.org/10.1007/BF00007865.
Lundh, F., 1999. An introduction to tkinter. URL: wwwpythonwarecom/library/tkinter/introduction/indexhtm.
Main, C.R., Doll, C., Bianco, C., Greenfield, D.I., Coyne, K.J., 2014. Effects of growth phase, diel cycle and macronutrient stress on the quantification of *Heterosigma akashiwo* using qPCR and SHA. Harmful Algae 37, 92–99. https://doi.org/10.1016/j.hal.2014.05.014.
Manso, S., 2014. Bioreceptivity optimisation of concrete substratum to stimulate biological colonisation. Tesi doctoral. UPC, Departament d'Enginyeria de la Construcció 2014. https://doi.org/10.5821/dissertation-2117-95324.
Manso, S., Aguado, A., 2016. The use of bio-receptive concrete as a new typology of living wall systems. Matériaux Tech. 104, 502. https://doi.org/10.1051/mattech/2016028.
Manso, S., Calvo-Torras, M.Á., De Belie, N., Segura, I., Aguado, A., 2015. Evaluation of natural colonisation of cementitious materials: effect of bioreceptivity and environmental conditions. Sci. Total Environ. 512–513, 444–453. https://doi.org/10.1016/j.scitotenv.2015.01.086.
Manso, S., De Muynck, W., Segura, I., Aguado, A., Steppe, K., Boon, N., De Belie, N., 2014. Bioreceptivity evaluation of cementitious materials designed to stimulate biological growth. Sci. Total Environ. 481, 232–241. https://doi.org/10.1016/j.scitotenv.2014.02.059.
Maury-Ramirez, A., Muynck, W., Stevens, R., Demeestere, K., De Belie, N., 2013. Titanium dioxide based strategies to prevent algal fouling on cementitious materials. Cement Concr. Compos. 36, 93–100. https://doi.org/10.1016/j.cemconcomp.2012.08.030.
Maxwell, K., Johnson, G.N., 2000. Chlorophyll fluorescence—a practical guide. J. Exp. Bot. 51, 659–668. https://doi.org/10.1093/jexbot/51.345.659.
Mckinney, W., 2010. Data structures for statistical computing in python. Proceedings of the 9th Python in Science Conference, pp. 56–61. https://doi.org/10.25080/Majora-92bf1922-00a.
Meng, S., Yang, R., Wu, J., Zhang, H., 2014. Simulation of droplet spreading on porous substrates using smoothed particle hydrodynamics. Int. J. Heat Mass Tran. 77, 828–833. https://doi.org/10.1016/j.ijheatmasstransfer.2014.05.056.
Miller, A.Z., Laiz, L., Dionísio, A., Macedo, M., Saiz-Jimenez, C., 2009. Growth of phototrophic biofilms from limestone monuments under laboratory conditions. Int. Biodeterior. Biodegrad. 63, 860–867. https://doi.org/10.1016/j.ibiod.2009.04.004.
Miller, A.Z., Sanmartín, P., Pereira-Pardo, L., Dionísio, A., Saiz-Jimenez, C., Macedo, M. F., Prieto, B., 2012. Bioreceptivity of building stones: a review. Sci. Total Environ. 426, 1–12. https://doi.org/10.1016/j.scitotenv.2012.03.026.
Najafpour, M., 2012. Applied Photosynthesis. InTech. https://doi.org/10.5772/2444.
Nielsen, H.D., Nielsen, S.L., 2008. Evaluation of imaging and conventional PAM as a measure of photosynthesis in thin- and thick-leaved marine macroalgae. Aquat. Biol. 3, 121–131. https://doi.org/10.3354/ab00069.
Nies, T., Niu, Y., Ebenhöh, O., Matsubara, S., Matuszyńska, A., 2021. Chlorophyll fluorescence: how the quality of information about PAM instrument parameters may affect our research. bioRxiv. https://doi.org/10.1101/2021.05.12.443801.
Nikolaou, A., Bernardi, A., Meneghesso, A., Bezzo, F., Morosinotto, T., Chachuat, B., 2015. A model of chlorophyll fluorescence in microalgae integrating photoproduction, photoinhibition and photoregulation. J. Biotechnol. 194, 91–99. https://doi.org/10.1016/j.jbiotec.2014.12.001.
Nilimaa, J., 2023. Smart materials and technologies for sustainable concrete construction. Dev. Built Environ. 15, 100177. https://doi.org/10.1016/j.dibe.2023.100177.
Oxborough, K., 2004. Imaging of chlorophyll a fluorescence: theoretical and practical aspects of an emerging technique for the monitoring of photosynthetic performance. J. Exp. Bot. 55, 1195–1205. https://doi.org/10.1093/jxb/erh145.
Pinheiro, A.C., Mesquita, N., Trovão, J., Soares, F., Tiago, I., Coelho, C., de Carvalho, H. P., Gil, F., Catarino, L., Piñar, G., Portugal, A., 2019. Limestone biodeterioration: a review on the Portuguese cultural heritage scenario. J. Cult. Herit. 36, 275–285. https://doi.org/10.1016/j.culher.2018.07.008.
Prieto, B., Paz-Bermúdez, G., López de Silanes, M.E., Montojo, C., Pérez-Velón, D., 2024. Current knowledge regarding biological recolonization of stone cultural heritage after cleaning treatments. J. Build. Eng. 87, 109091. https://doi.org/10.1016/j.jobe.2024.109091.
Proença, M. da C., Barbosa, M., Amorim, A., 2022. Counting microalgae cultures with a stereo microscope and a cell phone using deep learning online resources. Bull. Natl. Res. Cent. 46, 278. https://doi.org/10.1186/s42269-022-00965-z.
Qiu, X., Shimaki, Y., Tsuyama, M., Yamada, T., Kuwara, R., Kawaguchi, M., Honda, M., Gunjikake, H., Tasmin, R., Shimizu, M., Sato, Y., Kato-Unoki, Y., Nakashimi, T., Matsubara, T., Yamasaki, Y., Ichinose, H., Wariishi, H., Honjo, T., Oshima, Y., 2013. Growth-phase dependent variation in photosynthetic activity and cellular protein expression profile in the harmful raphidophyte *Chattonella antiqua*. Biosci. Biotechnol. Biochem. 77, 46–52. https://doi.org/10.1271/bbb.120543.
Romeu, M.J.L., Domínguez-Pérez, D., Almeida, D., Morais, J., Campos, A., Vasconcelos, V., Mergulhão, F.J.M., 2020. Characterization of planktonic and biofilm cells from two filamentous Cyanobacteria using a shotgun proteomic approach. Biofouling 36, 631–645. https://doi.org/10.1080/08927014.2020.1795141.
Rosenqvist, E., van Kooten, O., 2003. Chlorophyll fluorescence: a general description and nomenclature. In: DeEll, J.R., Toivonen, P.M.A. (Eds.), Practical Applications of Chlorophyll Fluorescence in Plant Biology. Springer, US, Boston, MA, pp. 31–77. https://doi.org/10.1007/978-1-4615-0415-3_2.
Rousso, B.Z., Bertone, E., Stewart, R., Aguiar, A., Chuang, A., Hamilton, D.P., Burford, M. A., 2022. Chlorophyll and phycocyanin in-situ fluorescence in mixed cyanobacterial species assemblages: effects of morphology, cell size and growth phase. Water Res. 212, 118127. https://doi.org/10.1016/j.watres.2022.118127.
Sanmartín, P., Grove, R., Carballeira, R., Viles, H., 2020a. Impact of colour on the bioreceptivity of granite to the green alga *Apatococcus lobatus*: laboratory and field testing. Sci. Total Environ. 745, 141179. https://doi.org/10.1016/j.scitotenv.2020.141179.
Sanmartín, P., Méndez, A., Carballeira, R., López, E., 2021a. New insights into the growth and diversity of subaerial biofilms colonizing granite-built heritage exposed to UV-A or UV-B radiation plus red LED light. Int. Biodeterior. Biodegrad. 161, 105225. https://doi.org/10.1016/j.ibiod.2021.105225.
Sanmartín, P., Miller, A.Z., Prieto, B., Viles, H.A., 2021b. Revisiting and reanalysing the concept of bioreceptivity 25 years on. Sci. Total Environ. 770, 145314. https://doi.org/10.1016/j.scitotenv.2021.145314.
Sanmartín, P., Rodríguez, A., Aguiar, U., 2020b. Medium-term field evaluation of several widely used cleaning-restoration techniques applied to algal biofilm formed on a granite-built historical monument. Int. Biodeterior. Biodegrad. 147, 104870. https://doi.org/10.1016/j.ibiod.2019.104870.
Sanmartín, P., Sanjurjo-Sánchez, J., Prieto, B., 2020c. Covering layers on granite buildings of Northwestern iberian peninsula: when observable characteristics and lab characterization do not match. Coatings 10, 137. https://doi.org/10.3390/coatings10020137.
Sanmartín, P., Vázquez-Nion, D., Arines, J., Cabo-Domínguez, L., Prieto, B., 2017. Controlling growth and colour of phototrophs by using simple and inexpensive coloured lighting: a preliminary study in the Light4Heritage project towards future strategies for outdoor illumination. Int. Biodeterior. Biodegrad. 122, 107–115. https://doi.org/10.1016/j.ibiod.2017.05.003.
Santo, A.P., Cuzman, O.A., Petrocchi, D., Pinna, D., Salvatici, T., Perito, B., 2021. Black on white: microbial growth darkens the external marble of florence cathedral. Appl. Sci. 11, 6163. https://doi.org/10.3390/app11136163.
Schagerl, M., Siedler, R., Konopáčová, E., Ali, S.S., 2022. Estimating biomass and vitality of microalgae for monitoring cultures: a roadmap for reliable measurements. Cells 11, 2455. https://doi.org/10.3390/cells11152455.
Schmitt-Jansen, M., Altenburger, R., 2008. Community-level microalgal toxicity assessment by multiwavelength-excitation PAM fluorometry. Aquat. Toxicol. 86, 49–58. https://doi.org/10.1016/j.aquatox.2007.10.001.
Schneider, C.A., Rasband, W.S., Eliceiri, K.W., 2012. NIH image to ImageJ: 25 years of image analysis. Nat. Methods 9, 671–675. https://doi.org/10.1038/nmeth.2089.
Schreiber, U., 2004. Pulse-Amplitude-Modulation (PAM) fluorometry and saturation pulse method: an overview. In: Papageorgiou, G.C., Govindjee (Eds.), Chlorophyll a Fluorescence: a Signature of Photosynthesis, Advances in Photosynthesis and Respiration. Springer, Netherlands, Dordrecht, pp. 279–319. https://doi.org/10.1007/978-1-4020-3218-9_11.
Schreiber, U., Schliwa, U., Bilger, W., 1986. Continuous recording of photochemical and non-photochemical chlorophyll fluorescence quenching with a new type of modulation fluorometer. Photosynth. Res. 10, 51–62. https://doi.org/10.1007/BF00024185.

Seabold, S., Perktold, J., 2010. Statsmodels: econometric and statistical modeling with Python. Proceedings of the 9th Python in Science Conference, pp. 92–96. https://doi.org/10.25080/Majora-92bf1922-011.

Singla, S., Harjai, K., Chhibber, S., 2014. Artificial *Klebsiella pneumoniae* biofilm model mimicking *in vivo* system: altered morphological characteristics and antibiotic resistance. J. Antibiot. 67, 305–309. https://doi.org/10.1038/ja.2013.139.

Sjollema, S.B., van Beusekom, S.A.M., van der Geest, H.G., Booij, P., de Zwart, D., Vethaak, A.D., Admiraal, W., 2014. Laboratory algal bioassays using PAM fluorometry: effects of test conditions on the determination of herbicide and field sample toxicity. Environ. Toxicol. Chem. 33, 1017–1022. https://doi.org/10.1002/etc.2537.

Stock, W., Blommaert, L., Daveloose, I., Vyverman, W., Sabbe, K., 2019. Assessing the suitability of Imaging-PAM fluorometry for monitoring growth of benthic diatoms. J. Exp. Mar. Biol. Ecol. 513, 35–41. https://doi.org/10.1016/j.jembe.2019.02.003.

Stohl, L., Manninger, T., Dehn, F., von Werder, J., 2025a. Understanding bioreceptivity of concrete: material design and characterization. Mater. Struct. 58, 335. https://doi.org/10.1617/s11527-025-02863-y.

Stohl, L., Manninger, T., von Werder, J., Dehn, F., Gorbushina, A., Meng, B., 2023. Bioreceptivity of concrete: a review. J. Build. Eng. 76, 107201. https://doi.org/10.1016/j.jobe.2023.107201.

Stohl, L., Tonon, C., Cook, J., Gorbushina, A., Dehn, F., von Werder, J., 2025b. Understanding bioreceptivity of concrete: realistic and accelerated weathering experiments with model subaerial biofilms. Mater. Struct. 59, 22. https://doi.org/10.1617/s11527-025-02864-x.

Thu Hien, T., Govin, A., Guyonnet, R., Grosseau, P., Lors, C., Garcia-Diaz, E., Damidot, D., Devès, O., Ruot, B., 2012. Influence of the intrinsic characteristics of mortars on biofouling by *Klebsormidium flaccidum*. Int. Biodeterior. Biodegrad. 70, 31–39. https://doi.org/10.1016/j.ibiod.2011.10.017.

Tonon, C., Breitenbach, R., Voigt, O., Turci, F., Gorbushina, A.A., Favero-Longo, S.E., 2021. Hyphal morphology and substrate porosity -rather than melanization- drive penetration of black fungi into carbonate substrates. J. Cult. Herit. 48, 244–253. https://doi.org/10.1016/j.culher.2020.11.003.

Tretiach, M., Bertuzzi, S., Salvadori, O., 2010. Chlorophyll a fluorescence as a practical tool for checking the effects of biocide treatments on endolithic lichens. Int. Biodeterior. Biodegrad. 64, 452–460. https://doi.org/10.1016/j.ibiod.2010.05.004.

Vázquez-Nion, D., Silva-Hermo, B., Prieto, B., 2018. Influence of the properties of granitic rocks on their bioreceptivity to subaerial phototrophic biofilms. Sci. Total Environ. 610–611, 44–54. https://doi.org/10.1016/j.scitotenv.2017.08.015.

Veeger, M., Ottelé, M., Prieto, A., 2021. Making bioreceptive concrete: formulation and testing of bioreceptive concrete mixtures. J. Build. Eng. 44, 102545. https://doi.org/10.1016/j.jobe.2021.102545.

Vieira, S., Ribeiro, L., Jesus, B., Cartaxana, P., Silva, J.M. da, 2013. Photosynthesis assessment in microphytobenthos using conventional and imaging pulse amplitude modulation fluorometry. Photochem. Photobiol. 89, 97–102. https://doi.org/10.1111/j.1751-1097.2012.01224.x.

Vijay, G., Gobinath, R., Binti Katman, H.Y., 2025. Global perspectives on sustainable concrete development: trends and future directions. Adv. Civ. Eng. 2025, 4123280. https://doi.org/10.1155/adce/4123280.

Villa, F., Stewart, P.S., Klapper, I., Jacob, J.M., Cappitelli, F., 2016. Subaerial biofilms on outdoor stone monuments: changing the perspective toward an ecological framework. Bioscience 66, 285–294. https://doi.org/10.1093/biosci/biw006.

von Werder, J., Venzmer, H., 2013. The potential of pulse amplitude modulation fluorometry for evaluating the resistance of building materials to algal growth. Int. Biodeterior. Biodegrad. 84, 227–235. https://doi.org/10.1016/j.ibiod.2012.03.009.

Wangpraseurt, D., Lichtenberg, M., Jacques, S.L., Larkum, A.W.D., Kühl, M., 2019. Optical properties of corals distort variable chlorophyll fluorescence Measurements1. Plant Physiol. 179, 1608–1619. https://doi.org/10.1104/pp.18.01275.

Xiao, J., Zou, S., Poon, C.S., Sham, M.L., Li, Z., Shah, S.P., 2025. We use 30 billion tonnes of concrete each year — here's how to make it sustainable. Nature 638, 888–890. https://doi.org/10.1038/d41586-025-00568-4.

Zhu, C., Wang, L., Wang, Bowen, Wang, Biao, Tang, M., Wang, X., Li, Q., Hu, Y., Zhang, B., 2023. Application and evaluation of a new blend of biocides for biological control on cultural heritages. Int. Biodeterior. Biodegrad. 178, 105569. https://doi.org/10.1016/j.ibiod.2023.105569.